LAWRENCE
LIVERMORE
NATIONAL
LABORATORY

LLNL-JRNL-840836

MRL/MpJ Mice Joints Exhibit Alternatively Activated Macrophage Phenotype in Response to ACL Rupture and Post-Traumatic Osteoarthritis Onset

J. L. McCool, A. Sebastian, N. R. Hum, S. P. Wilson, D. K. Murugesh, B. Amiri, B. A. Christiansen, G. G. Loots

October 5, 2022

PlosONE

Disclaimer

PLOS ONE

CD206+Trem2+ Macrophage Accumulation in the Murine Knee Joint After Injury is Associated with Protection Against Post-Traumatic Osteoarthritis in MRL/MpJ Mice

--Manuscript Draft--

Manuscript Number:	
Article Type:	Research Article
Full Title:	CD206+Trem2+ Macrophage Accumulation in the Murine Knee Joint After Injury is Associated with Protection Against Post-Traumatic Osteoarthritis in MRL/MpJ Mice
Short Title:	MRL/MpJ mice elicit a strong macrophage response post knee injury.
Corresponding Author:	Gabriela G Loots University of California Davis Sacramento, CA UNITED STATES
Keywords:	Osteoarthritis; Cartilage; PTOA; Joint; Knee; Macrophage; scRNA-seq; Inflammation; ACL; Trem2; MRL/MpJ; C57BL/6J
Abstract:	Post-traumatic osteoarthritis (PTOA) is a painful joint disease characterized by the degradation of bone, cartilage, and other connective tissues in the joint. PTOA is initiated by trauma to joint-stabilizing tissues, such as the anterior cruciate ligament, medial meniscus, or by intra-articular fractures. In humans, ~50% of joint injuries progress to PTOA, while the rest spontaneously resolve. To better understand molecular programs contributing to PTOA development or resolution, we examined injury-induced fluctuations in immune cell populations and transcriptional shifts by single-cell RNA sequencing of synovial joints in PTOA-susceptible C57BL/6J (B6) and PTOA-resistant MRL/MpJ (MRL) mice. We identified significant differences in monocyte and macrophage subpopulations between MRL and B6 joints. A potent myeloid-driven anti-inflammatory response was observed in MRL injured joints that significantly contrasted the pro-inflammatory signaling seen in B6 joints. Multiple CD206+ macrophage populations classically described as M2 were found enriched in MRL injured joints. These CD206+ macrophages also robustly expressed Trem2, a receptor involved in inflammation and myeloid cell activation. These data suggest that the PTOA resistant MRL mouse strain displays an enhanced capacity of clearing debris and apoptotic cells induced by inflammation after injury due to an increase in activated M2 macrophages within the synovial tissue and joint space.
Order of Authors:	Jillian L McCool, Ph.D
	Aimy Sebastian, Ph.D
	Nicholas R Hum, Ph.D
	Stephen P Wilson, Ph.D
	Oscar A Davalos, Ph.D
	Deepa K Murugesh, B.S.
	Beheshta Amiri, B.S.
	Cesar Morfin, Ph.D
	Blaine A Christiansen, Ph.D
	Gabriela G Loots
Opposed Reviewers:	
Additional Information:	
Question	**Response**
Financial Disclosure Enter a financial disclosure statement that	Yes

describes the sources of funding for the work included in this submission. Review the submission guidelines for detailed requirements. View published research articles from *PLOS ONE* for specific examples. This statement is required for submission and **will appear in the published article** if the submission is accepted. Please make sure it is accurate. **Funded studies** Enter a statement with the following details: • Initials of the authors who received each award • Grant numbers awarded to each author • The full name of each funder • URL of each funder website • Did the sponsors or funders play any role in the study design, data collection and analysis, decision to publish, or preparation of the manuscript? Did you receive funding for this work?	
Please add funding details. as follow-up to "**Financial Disclosure** Enter a financial disclosure statement that describes the sources of funding for the work included in this submission. Review the submission guidelines for detailed requirements. View published research articles from *PLOS ONE* for specific examples. This statement is required for submission and **will appear in the published article** if the submission is accepted. Please make sure it is accurate.	Department of Defense Awards PR180268, PR180268P1 and PR192271. National Institute of Health grant R01 AR075013.

Funded studies Enter a statement with the following details: • Initials of the authors who received each award • Grant numbers awarded to each author • The full name of each funder • URL of each funder website • Did the sponsors or funders play any role in the study design, data collection and analysis, decision to publish, or preparation of the manuscript? Did you receive funding for this work?"	
Please select the country of your main research funder (please select carefully as in some cases this is used in fee calculation). as follow-up to "**Financial Disclosure** Enter a financial disclosure statement that describes the sources of funding for the work included in this submission. Review the submission guidelines for detailed requirements. View published research articles from *PLOS ONE* for specific examples. This statement is required for submission and **will appear in the published article** if the submission is accepted. Please make sure it is accurate. **Funded studies** Enter a statement with the following details: • Initials of the authors who received each award • Grant numbers awarded to each author • The full name of each funder • URL of each funder website • Did the sponsors or funders play any role in the study design, data collection and analysis, decision to publish, or preparation of the manuscript? Did you receive funding for this work?"	UNITED STATES - US
Competing Interests	The authors have declared that no competing interests exist.

Use the instructions below to enter a competing interest statement for this submission. On behalf of all authors, disclose any competing interests that could be perceived to bias this work—acknowledging all financial support and any other relevant financial or non-financial competing interests. This statement is required for submission and **will appear in the published article** if the submission is accepted. Please make sure it is accurate and that any funding sources listed in your Funding Information later in the submission form are also declared in your Financial Disclosure statement. View published research articles from *PLOS ONE* for specific examples. **NO authors have competing interests** Enter: *The authors have declared that no competing interests exist.* **Authors with competing interests** Enter competing interest details beginning with this statement: *I have read the journal's policy and the authors of this manuscript have the following competing interests: [insert competing interests here]* * typeset	
Ethics Statement Enter an ethics statement for this submission. This statement is required if the study involved: • Human participants • Human specimens or tissue • Vertebrate animals or cephalopods • Vertebrate embryos or tissues	All animal work was conducted in accordance to IACUC standards at LLNL and UCD. Details on animal studies are in Material and Methods section.

• Field research Write "N/A" if the submission does not require an ethics statement. General guidance is provided below. Consult the submission guidelines for detailed instructions. **Make sure that all information entered here is included in the Methods section of the manuscript.**	

Format for specific study types **Human Subject Research (involving human participants and/or tissue)** • Give the name of the institutional review board or ethics committee that approved the study • Include the approval number and/or a statement indicating approval of this research • Indicate the form of consent obtained (written/oral) or the reason that consent was not obtained (e.g. the data were analyzed anonymously) **Animal Research (involving vertebrate animals, embryos or tissues)** • Provide the name of the Institutional Animal Care and Use Committee (IACUC) or other relevant ethics board that reviewed the study protocol, and indicate whether they approved this research or granted a formal waiver of ethical approval • Include an approval number if one was obtained • If the study involved *non-human primates*, add *additional details* about animal welfare and steps taken to ameliorate suffering • If anesthesia, euthanasia, or any kind of animal sacrifice is part of the study, include briefly which substances and/or methods were applied **Field Research** Include the following details if this study involves the collection of plant, animal, or other materials from a natural setting: • Field permit number • Name of the institution or relevant body that granted permission	
Data Availability Authors are required to make all data underlying the findings described fully available, without restriction, and from the time of publication. PLOS allows rare exceptions to address legal and ethical concerns. See the PLOS Data Policy and FAQ for detailed information.	Yes - all data are fully available without restriction

A Data Availability Statement describing where the data can be found is required at submission. Your answers to this question constitute the Data Availability Statement and **will be published in the article**, if accepted. **Important:** Stating 'data available on request from the author' is not sufficient. If your data are only available upon request, select 'No' for the first question and explain your exceptional situation in the text box. Do the authors confirm that all data underlying the findings described in their manuscript are fully available without restriction?	
Describe where the data may be found in full sentences. If you are copying our sample text, replace any instances of XXX with the appropriate details. • If the data are **held or will be held in a public repository**, include URLs, accession numbers or DOIs. If this information will only be available after acceptance, indicate this by ticking the box below. For example: *All XXX files are available from the XXX database (accession number(s) XXX, XXX.*). • If the data are all contained **within the manuscript and/or Supporting Information files**, enter the following: *All relevant data are within the manuscript and its Supporting Information files.* • If neither of these applies but you are able to provide **details of access elsewhere**, with or without limitations, please do so. For example: *Data cannot be shared publicly because of [XXX]. Data are available from the XXX Institutional Data Access / Ethics Committee (contact via XXX) for researchers who meet the criteria for access to confidential data.* *The data underlying the results presented in the study are available from (include the name of the third party*	The datasets generated for this study can be found in the Gene Expression Omnibus (GEO) under accession numbers GSE200843 and GSE220167.

and contact information or URL). • This text is appropriate if the data are owned by a third party and authors do not have permission to share the data. * typeset	
Additional data availability information:	Tick here if the URLs/accession numbers/DOIs will be available only after acceptance of the manuscript for publication so that we can ensure their inclusion before publication.

CD206^{+} Trem2^{+} Macrophage Accumulation in the Murine Knee Joint After Injury is Associated with Protection Against Post-Traumatic Osteoarthritis in MRL/MpJ Mice

Jillian L. McCool[1,2], Aimy Sebastian[1], Nicholas R. Hum[1], Stephen P. Wilson[1], Oscar A. Davalos[1], Deepa K. Murugesh[1], Beheshta Amiri[1], Cesar Morfin[1,3], Blaine A. Christiansen[3], Gabriela G. Loots[1,2,3*]

[1]Lawrence Livermore National Laboratory, Physical and Life Science Directorate, Livermore, CA.

[2]University of California Merced, School of Natural Sciences, Merced, CA.

[3]University of California Davis Health, Department of Orthopaedic Surgery, Sacramento, CA.

[1]Biology and Biotechnology Division,

Lawrence Livermore National Laboratory

7000 East Avenue, L-452

Livermore, CA 94551

*Author for correspondence (e-mail: gloots@ucdavis.edu)

Disclosure

Authors have nothing to disclose.

Abstract

Post-traumatic osteoarthritis (PTOA) is a painful joint disease characterized by the degradation of bone, cartilage, and other connective tissues in the joint. PTOA is initiated by trauma to joint-stabilizing tissues, such as the anterior cruciate ligament, medial meniscus, or by intra-articular fractures. In humans, ~50% of joint injuries progress to PTOA, while the rest spontaneously resolve. To better understand molecular programs contributing to PTOA development or resolution, we examined injury-induced fluctuations in immune cell populations and transcriptional shifts by single-cell RNA sequencing of synovial joints in PTOA-susceptible C57BL/6J (B6) and PTOA-resistant MRL/MpJ (MRL) mice. We identified significant differences in monocyte and macrophage subpopulations between MRL and B6 joints. A potent myeloid-driven anti-inflammatory response was observed in MRL injured joints that significantly contrasted the pro-inflammatory signaling seen in B6 joints. Multiple $CD206^{+}$ macrophage populations classically described as M2 were found enriched in MRL injured joints. These $CD206^{+}$ macrophages also robustly expressed *Trem2*, a receptor involved in inflammation and myeloid cell activation. These data suggest that the PTOA resistant MRL mouse strain displays an enhanced capacity of clearing debris and apoptotic cells induced by inflammation after injury due to an increase in activated M2 macrophages within the synovial tissue and joint space.

Keywords: Osteoarthritis; Cartilage; PTOA; Joint; Knee; Macrophage; scRNA-seq; Inflammation; ACL; Trem2; MRL/MpJ; C57BL/6J

Introduction

In humans, nearly half of traumatic knee joint injuries progress to post-traumatic osteoarthritis (PTOA), while the remainder spontaneously resolve without progressive cartilage degeneration, independent of whether corrective surgery occurs. The pathogenesis and onset of the PTOA are still not fully understood, but multiple factors such as genetics, epigenetics, and immune responses have been implicated in disease progression [1]. This study examined the immune system's responses to anterior crucial ligament (ACL) injury in C57BL/6J (B6), a PTOA vulnerable mouse strain and 'super-healer' MRL/MpJ (MRL) mice that are resistant to PTOA [2] to better understand the immune-driven mechanisms of resistance to joint degeneration. The MRL strain has been described to have an extraordinary capacity for regenerating soft tissues after damage, as well as repairing injured cartilage [2-10]. In a noninvasive tibial compression injury model, our group previously showed that MRL joints remain resistant to cartilage degradation for at least 12 weeks post injury, the latest time point examined [9]. These injured MRL joints also developed significantly less osteophyte formation and displayed comparable OARSI scores to uninjured controls, indicating a non-arthritic joint resolution post injury [9]. While the MRL joint has been histologically evaluated, cellular and molecular interactions leading to this resistant phenotype have not yet been fully elucidated.

The timeline of PTOA progression following joint injury can be classified into several phases starting at trauma. After the immediate sequelae of injury, an acute/subacute phase, dominated by inflammation, leukocyte infiltration, and tissue remodeling occurs. This inflammatory phase can spontaneously resolve after a few weeks or months, or progress to a chronic phase that can last for years, during which metabolic changes in the tissue progress through a clinically asymptomatic

period that eventually leads to PTOA with severe joint pain and restricted mobility [11] that may become debilitating without surgical intervention [12].

An increasing number of studies have shown that arthritis progression is dependent on the immune system's response to injury [13-17] and have implicated multiple immune cell types including macrophages, monocytes, neutrophils, dendritic cells, B and T cells in the pathogenesis of osteoarthritis [18-20]. Macrophages are the major immune cell type present in healthy synovial tissues of the joint; they are essential in maintaining the integrity of the synovial cavity to keep articular cartilage unperturbed by endogenous damage-associated molecular patterns (DAMPs) that form from wear and tear of the joint [21]. During acute inflammation, as in the case of injury, there is an increase in monocytes, activated macrophages, and synovial fibroblasts that enter the joint space due to a disruption of the synovial lining [22, 23]. This influx leads to an expansion of the synovial pannus and degradation of the articular cartilage due to a spike in metalloproteinases secreted by infiltrating monocyte-derived macrophages [24]. Some subpopulations such as the *Trem2*$^{+}$ (Triggering Receptor Expressed On Myeloid Cells 2) alternatively activated macrophages have been described as anti-inflammatory and are likely to promote healing and repair of damaged tissues [25-27]. Previously, we identified *Trem2*$^{+}$ macrophages as a major subpopulation in B6 mice that expands in response to knee injury [28]. Characterizing key cell types like Trem2^{+} macrophages that prompt an anti-inflammatory phenotype is crucial in understanding immune cell function that aids healing and prevents PTOA development, post injury. Additionally, these subpopulations have clinical relevance as potential cell-based therapies where macrophages of appropriate phenotypes can directly improve healing or enable the production of macrophage-derived therapeutic proteins for long term damage control.

To enhance our understanding of the role the immune system plays in PTOA progression we employed single-cell RNA sequencing (scRNA-seq) analysis of injured and uninjured knee joints from MRL and B6, which allowed us to characterize tissue resident and infiltrating immune cell populations. We were able to highlight significant differences in myeloid subpopulations in the synovial capsule and infrapatellar fat pad of MRLs after injury. The immune characterization of 'PTOA-resistant' MRL and 'PTOA-vulnerable' B6 joints presented here identified several strain-specific differences that correlate with a disease protection phenotype and should be further explored mechanistically and therapeutically.

Materials and Methods

Experimental Animals and ACL Injury Model

MRL (MRL/MpJ, Stock # 000486) and B6 (C57BL/6J, Stock # 000664) animals were purchased from Jackson Laboratory and bred in house using standard procedures. Ten-week-old male MRL and B6 were anesthetized using isoflurane inhalation and subjected to non-invasive knee joint injury as previously described [29]. Briefly, the right lower leg was placed between two platens and was subjected to single tibial compression overload (~10-16N) at 1 mm/s displacement rate to induce an ACL rupture using an electromagnetic material testing system (ElectroForce 3200, TA Instruments, New Castle, DE, USA). Mice were administered a 50 µL dose of 0.9% sterile saline (Becton, Dickinson and Company, Franklin Lakes, NJ, USA), and a body mass dependent dose of buprenorphine (0.01 mg/kg) immediately post-injury for pain relief. Mice were then allowed normal cage activity while on 12h light/dark cycles prior to euthanasia at terminal time points. All animal experimental procedures were completed in accordance with the Institutional Animal Care and Use Committee (IACUC) guidance at Lawrence Livermore National Laboratory and the University of California, Davis in AAALAC-accredited facilities.

Histological assessment of the articular joint

After ACL injury, right hindlimbs (n=5/group) were collected from uninjured day 0 (D0) and injured mice at day 7 (D7) and 4 weeks (4W) post-injury and processed for histological evaluation as previously described [28]. Briefly, whole hindlimbs were fixed in 10% Neutral Buffered Formalin (NBF), decalcified using 0.5 M EDTA using the weight loss-weight gain method for measuring decalcification status [30] and processed for paraffin embedding. Joints were sectioned in the sagittal plane at 6 µm and serial medial sections were prepared for histological assessment of joint tissue integrity at all timepoints. Sections were stained on charged glass slides using 0.1% Safranin-O (0.1%, Sigma, St. Louis, MO, USA; S8884) and 0.05% Fast Green (0.05%, Sigma, St. Louis, MO, USA; F7252) using standard procedures (IHC World, Woodstock, MD, USA). Slides were imaged using a Leica DM5000 microscope (Leica Microsystems, Wetzlar, Germany). ImagePro Plus V7.0 Software, a QIClick CCD camera (QImaging, Surrey, BC, Canada), and ImageJ V1.53 Software were used for imaging and photo editing [31]

OARSI Histological Scoring of Joint Degradation

Serial medial sections from B6 and MRL (n=5/strain) were stained using Safranin-O and Fast Green as described above and subjected to a blinded semi-quantitative scoring by five individual scientists using the OARSI Histopathology Scoring System [32]. All scores were averaged and mean score was plotted to determine the grade of joint damage that had occurred at 4W post injury.

Immunohistochemistry

Serial medial sections from B6 and MRL (n=5/strain) were subjected to antigen retrieval with Unitrieve (NB325 Innovex Biosciences, Richmond, CA. USA) and blocking using Background Buster (NB306 Innovex Biosciences, Richmond, CA. USA) per manufacturer's instructions.

Samples were stained with primary antibodies and incubated overnight at 4°C in a dark, humid chamber. Samples were washed and incubated for 2 hours at room temperature in a dark, humid chamber with secondary antibodies at 1:500. Negative control slides were incubated with secondary antibody only. Stained slides were mounted with Prolong Gold with DAPI for nuclei staining (Molecular Probes, Eugene, OR. USA). Slides were imaged using a Leica DM5000 microscope. ImagePro Plus V7.0 Software, QIClick CCD camera (QImaging, Surrey, BC, Canada) and ImageJ V1.53 Software were used for imaging and photo editing. Primary antibodies included: Trem2 [1:100; ab95470 Abcam, Cambridge, UK], CD206 [1:100; ab64693, Abcam, Cambridge, UK], S100a8 [1:100; ab92331 Abcam, Cambridge, UK], Lyve1 [1:100; ab218535 Abcam, Cambridge, UK], Ly6G [1:100; ab238132 Abcam, Cambridge, UK]. Secondary antibodies included goat anti-rabbit 594 (1:1000; A11037, Thermofisher, Waltham, MA. USA), donkey anti-goat 488 (1:1000; A11055, ThermoFisher, Waltham, MA. USA).

Single cell RNA sequencing (scRNA-seq)

D0 (uninjured) and joints ($n \geq 4$/time point/strain) from day 1 (D1), D3, D7, 2 weeks (2W), and 4W post-injury were collected from MRL and B6 mice for scRNA-seq analysis. Mice were euthanized humanely under CO_2 and entire hindlimbs were dissected free of any superficial tissues such as the muscle, retaining the synovial fluid between the tibia and femur. To obtain immune cells from the joint without any bone marrow contamination, joint-residing cells from intact joints were released by digesting the soft tissues around the joint. Cells residing in the synovial capsule were collected by separating the joint between the femur and tibia into 7.5 mL of DMEM/F12 containing 3% Collagenase 1 solution (Worthington Biochemical, Lakewood, NJ; CLS-1) and 100 µg/mL DNase I (Roche, Basel, Switzerland; 11284932001). Hindlimbs with joint tissues were then digested while shaking at 37°C for two 1-hour digests and then filtered through a 100µm nylon cell strainer to

remove large tissue fragments. After digestion, red blood cell lysis was performed with ammonium-chloride-potassium (ACK) lysis buffer (ThermoFisher Scientific, Waltham, MA, USA; A1049201) then CD45+ immune cells were enriched using CD45-conjugated magnetic microbeads (Miltenyi Biotech, Bergisch Gladbach, Germany; 130-052-301) followed by Miltenyi Biotech MACS separation with LC columns. For bone marrow cell isolation, femur and tibia were first isolated from uninjured, 10-week-old male BL6 mice. The bones were then gently crushed to expose the marrow cavity and thoroughly rinsed with PBS until all the marrow was flushed out of the bone. Bone marrow cells were then pelleted, and ACK red blood cell lysis was performed. All final cell preparations were resuspended in PBS with 1% FBS for scRNA-seq preparation. Each scRNA-seq sample was comprised of pooled 3-5 mouse replicates to mitigate biological variability. Immune ($CD45^+$) joint populations were sequenced using a Chromium Single Cell 3' V3 Reagent Kit and Chromium instrument (10x Genomics, Pleasanton, CA). Library preparation was performed according to the manufacturer's protocol and sequenced on an Illumina NextSeq 500 (Illumina, San Diego, CA, USA).

ScRNA-seq data analysis

Raw scRNA-seq data were processed using the Cell Ranger software (10x Genomics, Pleasanton, CA, USA) as described before [28]. Raw count matrices generated with Cell Ranger were loaded into R (v4.3.2) and merged into a single object for downstream analysis using Seurat (v4.3.0) [33]. Cells were retained based on the following filtering criteria: number of counts ≥ 500; number of genes ≥ 200; mitochondrial gene percentage < 10. Genes expressed in less than 10 cells were removed. Data was normalized using the `NormalizeData` function with default parameters. Three thousand highly variable genes (HVGs) were identified using the "vst" method. Before dimension reduction the data was scaled using only HVGs with following variables regressed out: number of

counts and mitochondrial percentage. After scaling principal component analysis (PCA) was performed and principal components (PCs) 1-50 were used for subsequent analysis. Data integration i.e. batch correction was performed using Harmony with the grouping variable being "orig.ident" which contained all individual samples [34]. Clusters were identified using `FindNeighbors` and `FindClusters` with the reduction parameter set to "harmony" and resolution 0.2 which was used for labeling the clusters. A non-linear dimensional reduction was then performed *via* uniform manifold approximation and projection (UMAP) with the following parameter modifications: reduction = "harmony"; umap.method = "uwot"; spread=4. Cluster marker genes were identified using `FindAllMarkers` with the parameter only.pos set to true. Monocytes and macrophages (Mono/Mac) and neutrophils were all extracted and analyzed further following the same methods as above with the following differences: Mono/Mac (2000 HVGs, 1-40 PCs, resolution 0.5); Neutrophils (2000 HVGs, 1:40 PCs, resolution 0.5). Differential gene expression analysis between mouse strains was conducted by isolating the relevant cell type, assigning subset identity to strain, and applying `FindAllMarkers` with only.pos set to true. For neutrophil subpopulations, gene ontology (GO) enrichment analysis was performed on up to 100 differentially expressed genes per cluster using clusterProfiler(v4.10.0) [35, 36]. For genes differentially expressed between MRL and B6 in specific macrophage subpopulations (log2FC > 0.25; FDR <0.05), GO analysis was performed using ToppGene Suite [37] and enrichment dot plots were generated using custom R scripts. Pathway and transcription factor activity inferences were performed and visualized with decoupleR (v2.8.0) and SCpubr (v2.0.2) [38, 39]. All data wrangling and analysis was performed in R (v4.3.2) using tidyverse (v2.0.0) functions. Data visualization leveraged tools already mentioned above and a mixture of khroma (v1.11.0), ggthemes (5.0.0), and Rcolorbrewer (v1.1.3) for color palettes [40, 41].

Neutrophils from D0 B6 joints were compared to those from D0 bone marrow (BM) isolates. BM immune scRNA-seq data was integrated with immune scRNA-seq data from D0 B6 joints using Seurat's anchor-based canonical correlation analysis (CCA) integration method. CCA integration was performed by identifying 2000 HVGs per dataset, followed by applying `SelectIntegrationFeatures`, `FindIntegrationAnchors`, and `IntegrateData` functions using default parameters. After CCA based integration data processing followed the steps previously described above.

Single cell trajectory analysis

Single cell pseudo-time trajectories of immune cell subpopulations were constructed with Monocle [42]. Following analysis of scRNA-seq data in the Seurat object format; the expression data, phenotype data, and feature data were extracted for constructing Monocle's "CellDataSet" object utilizing the "newCellDataSet" function. Highly variable genes from within the Seurat object were selected as ordering genes. The Monocle "reduceDimension" function was used to reduce the dataset's dimensionality using the DDR algorithm. Ordering of cells along the computed trajectory was carried out using the "orderCells" function with default parameters.

Perfusion of mice

For the perfusion of blood, mice were anesthetized by administering isoflurane (4-5% in 100% oxygen *via* a nose cone. Once mice were no longer responsive to tail pinch reflex, the thoracic cavity was opened through the diaphragm, and ribs were cut bilaterally to expose the heart. A butterfly needle was then inserted into the left ventricle and secured. Next, a small incision was made in the right atrium to create an outlet for effluent. With the aid of a perfusion pump (flow set at 10ml/min), mice were perfused with 20ml of sterile PBS + 0.1% heparin.

Flow cytometry analysis

Single cell suspensions from injured and uninjured knee joints were generated as described above in the scRNA-seq section (n=3-5/group). Cells were blocked using rat anti-mouse CD16/CD32 (Stock # 14-0161-82, Mouse Fc Block; Thermo Fisher, Waltham, MA. USA) at 4^{o}C for 10 minutes then incubated with an antibody cocktail (Thermo Fisher) specific for macrophage characterization containing the following antibodies at a 1:100 dilution: PerCP CD45 monoclonal antibody (Clone: EM-05, Stock# MA110234), eFluor 506 CD11b monoclonal antibody (Clone: M1/70, Stock# 69-0112-82), PE F4/80 monoclonal antibody (Clone: QA17A29, Stock 157304), APC CD206/MMR monoclonal antibody (Clone: MR6F3, Stock# 17-2061-82), FITC TREM2 monoclonal antibody (Clone: 78.18, Stock# MA528223) and DAPI for viability staining. To identify proportions of myeloid cells, isolated cells from the knee joints at all timepoints were stained using Biolegend antibodies at 1:100 dilution: APC/Cy7 anti-mouse CD45 antibody (Clone: 30-F11), FitC anti-mouse/human CD11b antibody (Clone: M1/70), Brilliant Violet 510 anti-mouse Ly-6C (Clone: HK1.4), APC anti-mouse Ly-6G (Clone: 1A8) and DAPI for viability staining. Flow cytometry was also performed on perfused mice and neutrophil populations were identified within the joint cell suspensions using the following antibodies (BioLegend, San Diego, CA USA): anti-mouse APC CD45 antibody (Clone: 30-F11), anti-mouse FITC CD11b (Clone: M1/70), and anti-mouse APC/Cyanine7 Ly6g (Clone: 1A8) at a 1:100 dilution in PBS +1% FBS and DAPI was used as a viability stain. All flow cytometric analyses were performed on a BD FACSMelody system.

Analysis software and statistical analysis

Statistical analyses were performed using GraphPad Prism (n=3-5 biological replicates per strain). A one-way ANOVA and post-hoc Bonferroni's Test were used to assess statistically significant differences of mean expression values. OARSI scoring is presented from 4 biological replicates per strain and scored by 5 individual scientists. A one-way ANOVA and post-hoc Bonferroni's Test

were used to assess statistically significant differences of mean expression values. µCT statistical analysis was performed using two-way ANOVA and Student's T-test with a two-tailed distribution, with two-sample equal variance (homoscedastic test). Post-hoc Bonferroni's Tests were used to assess statistically significant differences of mean expression values. All results were considered statistically significant for *p*-values <0.05.

Results

ScRNA-seq reveals differences in knee joint immune landscape after injury in MRL and B6 mice.

Consistent with prior reports [6, 43-45], B6 mice showed visible proteoglycan loss, fibrillation, and significant erosion to the calcified cartilage layer by 4W post injury, while injured MRLs retained their pre-injury cartilage thickness with non-significant decreases in proteoglycan staining (**Figure 1A, B**). Single cell analysis of immune ($CD45^+$) cells from uninjured (D0), and D1, D3, D7, 2W, and 4W post injury joints identified changes in the immune profile of B6 and MRL mice before and after knee injury (**Figure 1C, D**). Seven immune cell clusters including: (1) Neutrophils, (2) Monocyte/Macrophages (Mono/Mac), (3) B cells, (4) Proliferating Neutrophils, (5) Proliferating Myeloid cells, (6) T/NK cells, and (7) Dendritic cells were identified and had specific changes to their populations over the injury time course (**Figure 1D-F**). All clusters were assigned identities based on the expression of known immune markers (**Figure 1F**). Specifically, cluster 1 was labeled as neutrophils due to high expression of *S100a8* and *S100a9*. Cluster 2 was labeled as monocytes/macrophages (Mono/Mac) due to high expression levels of *Csfr1*, *Cd14* and *Adgre1*. Cluster 3 was labeled B cells for robust expression of *Ighm*, *Cd19* and *Cd79a*. Clusters 4 and 5 were high in makers of proliferation and cell cycle (*Top2a*, *Mki67*) and cytoskeleton rearrangement (*Stmn1*, *Tubb*), and were classified as proliferating neutrophils and myeloid, respectively based on their distinct expression of neutrophil markers *S100a8/9* in 4 and macrophage marker *Csfr1* in 5.

T/NK cells clustered together in population 6 and were labeled based on their expression of *Nkg7* and *Thy1*. Lastly, cells in cluster 7 were classified as dendritic cells due to their high expression of *Siglech* and *Ccr9* (**Figure 1F**).

Figure 1. Assessment of changes associated with PTOA onset in MRL and B6. *(A) PTOA resistant MRL (top row) showed little loss of staining after injury in the articular cartilage of the femur and tibia (red) indicating little to no loss of proteoglycan content in the cartilage matrix (top right, * asterisk). PTOA susceptible B6 (bottom row) showed severe degradation of bone (blue,) and cartilage (red) in the tibia, and loss of some cartilage in the femur after injury (bottom right, ▲ triangle). Scale bar = 100µm. Magnification 20X. F-Femur, T-Tibia. n=5 / group. (B) Blinded OARSI scoring of uninjured (D0) and injured (4W) B6 and MRL joints. (*** p<0.001; ****p<0.0001). (C) Schematic of the scRNA-seq pipeline. Uninjured murine joints were collected at Day 0 (D0), injured joints were collected at Days 1- (D1), 3- (D3), 7- (D7) days, 2- (2W) and 4- (4W) weeks following tibial compression and all prepared for scRNA-seq. Digested immune cells (CD45+) were enriched before conducting scRNA-seq. (D) Uniform Manifold Approximation and Projection (UMAP) plot representing seven immune cell types within the synovial joint at all timepoints examined. (E) UMAP plot from panel D colored based on experimental groups. (F) Dot plots identifying specific markers for each cell type. Size of the dot indicates cellular abundance and color indicates expression.*

In uninjured joints, the proportion of the immune cell population represented by neutrophils was the largest in both strains, accounting for 58.7% and 71.9% of the total immune cells sequenced in B6 and MRL, respectively (**Figure 2A**). The remainder of the populations segregated as follows in uninjured B6 and MRLs: 10.1% and 9.1% Mono/Macs, 18.8% and 7.6% B cells, 3% and 3.5%

proliferating myeloid, 5.3% and 3.5% proliferating neutrophils; 3% and 3.9% T/NK; ~1% and 0.5% dendritic cells. After injury, strain specific trends were observed for several cell types, with the largest population shifts occurring at D3 for nearly all identified cell types (**Figure 2A, Table S1**). Prior to injury, the Mono/Mac populations were comparable in both strains, but a significant shift was observed at D3 post injury, where the proportion of these cells increased to 62.4% in MRL, and 35.5% in B6, then decreased by D7 (**Figure 2A, Table S1**). At D3, the proportion of neutrophils sequenced decreased by 48.5% and 14.2% from baseline levels, in MRL and B6, respectively (**Figure 2A**). Additionally, the proportion of total proliferating myeloid cells increased by 5.2% from baseline in MRL, and 2.4% in B6 (**Table S1**).

Figure 2. Time course of immune cell population changes post injury. *(A) Percent of total for each immune population identified through scRNA-seq, determined as a proportion of all immune cells sequenced. Colors based on immune cluster identities denoted in Fig. 1D. (B) Flow cytometry gating strategy for Ly6c+ monocytes/macrophages (Mono/Mac) and neutrophil populations. (C) Trend of* $Ly6c^+$ *monocytes and macrophages after injury. (D) Trend of* $Ly6g^+$ *neutrophils after injury.*

Since neutrophils and Mono/Macs showed the most dramatic population shifts and strain differences after injury, we focused our analysis on these two cell types. Flow cytometry confirmed that the proportion of $CD45^+CD11b^+Ly6c^+$ Mono/Macs in the synovial joint gradually increased in both strains, peaking at D3, and returning close to pre-injury levels by 4W (**Figure 2B, C**). A corresponding decrease in neutrophils was also observed by flow cytometry (**Figure 2B, D**). We also noted that MRLs had a significantly higher proportion of Mono/Macs at D1, D3 and D7 compared to B6 while B6 mice had more neutrophils than MRL specifically at D3 (**Figure 2A, C, D**).

Neutrophils display strain specific changes in response to knee injury.

Neutrophils were the major immune cell type identified in both MRL and B6 joints. These cells showed enrichment for several immune modulators including *Il1b*, a key cytokine implicated in osteoarthritis pathogenies and *Csf1*, a key regulator of monocyte to macrophage differentiation (**Figure 2A, D, S1A**). To rule out the possibility that the neutrophils identified in the single cell digests were from circulation and determine whether the decrease in neutrophil proportion observed after injury corresponds to a true reduction in total neutrophils or is merely a consequence of an increase in infiltrating cells, such as Mono/Macs, flow cytometry was performed following perfusion on an additional cohort of B6. The absolute and relative number of neutrophils was analyzed at D0 and D6 post injury. We found neutrophils to contribute to ~70% of the immune cells at D0 after perfusion and a reduction in the proportion of neutrophils was observed at D6 compared to D0 *via* flow cytometric analysis (**Figure 3A**). However, our analysis showed that the total neutrophil counts were not significantly different between D0 and D6 joints (**Figure 3B**), suggesting that the reduction in the relative proportion of neutrophils after injury is likely due to infiltration of other immune cells into the joint.

Figure 3. Injury induced changes in MRL and B6 neutrophils. *A) Flow cytometry data showing the abundance of neutrophils relative to total immune cells in the knee joint digest after perfusion. B) Flow cytometry data showing the absolute counts of neutrophils in the knee joint digest after perfusion. C) UMAP plot showing the neutrophil subpopulations identified by scRNA-seq. D) Feature plots showing key markers of various neutrophil subpopulations. E) Changes in the proportion of various neutrophil subpopulations in response to injury in B6 and MRL, relative to total immune cells sequenced. F) Dot plot showing ontology processes enriched in each neutrophil subtype. G) Heatmap showing key genes differentially expressed between neutrophil subpopulations and between mouse strains.*

Neutrophils are highly heterogeneous with several developmental stages [46]. Re-clustering of all neutrophils (cluster 1 in Figure 1D) identified four subtypes with distinct transcriptional profiles: (1) *Ccrl2*$^{+}$ neutrophils which showed strong enrichment for *Il1b*; (2) *Mmp8*$^{+}$ neutrophils; (3) *Chil3*$^{+}$ neutrophils and (4) *IfnR*$^{+}$ neutrophils (**Figure 3C-D, S1B-C**). Relative proportions of all neutrophil subtypes were lower in MRL at D3 compared to BL6 (**Figure 3E**). Furthermore, gene expression signatures of *Chil3*$^{+}$ neutrophils (*Chil3*, *Cebpe*, *Ngp*, *Ltf*, *Cd177*) correlated with previously established signatures of immature neutrophils while genes enriched in *Ccrl2*$^{+}$ and *IfnR*$^{+}$ neutrophils (*Ccl6*, *Csf3r*, *Il1b*, *Fth1*, *Ifitm1*, *Ifitm2*, *Btg1*, *Srgn*, *Msrb1*) correlated with mature neutrophils. *Mmp8*$^{+}$ neutrophils had a signature (*Mmp8*, *Lgals3*, *Retnlg*) of an intermediate stage of neutrophil differentiation [47] (**Figure S1C, Table S2**). A gene ontology analysis identified enrichment of 'neutrophil activation' related genes in *Mmp8*$^{+}$ and *Chil3*$^{+}$ neutrophils while *Ccrl2*$^{+}$ neutrophils showed enrichment for processes such as 'cell migration' and 'response to chemokines' (**Figure 3F**).

Further analysis of differentially expressed genes between various neutrophil subtypes showed that *Ccrl2*$^{+}$ and *IfnR*$^{+}$ neutrophils in B6 joints expressed higher levels of inflammatory cytokines, including *Il1β*, *Tnf* and *Il15*, when compared to MRL. Meanwhile, *Il18rap*, *Mmp9* and *Il1rn*, an endogenous IL1 receptor antagonist, [48] were highly expressed in MRL joints (**Figure 3G, Table S3**). MRL joints also had increased expression of *Csf1*, a critical regulator of macrophage differentiation, when compared to B6 (**Figure S1D**).

Although neutrophils constituted ~70% of immune cells at D0 in both our scRNA-seq and flow cytometry data, immunohistochemical analysis of joint tissue sections only showed a substantial number of cells expressing neutrophil markers S100a8 or Ly6g in the joint *after* injury (**Figure S2A-B**). To determine if the neutrophils in our digests were bone marrow-derived, we

computationally compared scRNA-seq derived transcriptome profiles of the neutrophil populations from the D0 synovial joint digest to BM derived neutrophils. Similar to synovial joints, *Ccrl2*$^{+}$, *Mmp8*$^{+}$, *Chil3*$^{+}$, *IfnR* and proliferating neutrophils were also detected in BM however, the synovial joint had a significantly higher proportion of mature *Ccrl2*$^{+}$ neutrophils while the BM had more proliferating and immature neutrophils (**Figure S2C-F**). We also found that synovial neutrophils expressed higher levels of inflammatory cytokines such as *Tnf*, *Il1β*, *Ccl3* and *Ccl4* when compared to BM derived neutrophils. BM derived neutrophils also showed enrichment for immature neutrophil markers *Elane*, *Mpo*, *Chil3*, *Lcn2* and *Ly6g* (**Figure S2G**) [47], suggesting that neutrophils from the joint have a different molecular profile than the BM neutrophils. Additionally, histological analysis of the digested synovial joint indicated that the bones remained intact after digestion while the soft tissue around the knee joint was completely digested (**Figure S2H**). This suggests that the neutrophils in our digest likely originate from tissues around the synovial joint and not from BM contamination.

Injured MRL joints harbor significantly more macrophages than B6 injured joints

The Mono/Mac population showed the most dramatic increase in both B6 and MRL after injury. To enhance our understanding of the roles that monocytes and macrophages have in PTOA onset, Mono/Mac cells from the single cell analysis were extracted and further analyzed to investigate strain-specific changes in these cell populations, longitudinally. Eleven subpopulations (**Figure 4A-B**) with distinct gene expression profiles (**Figure 4C, Table S4**) were identified; all cells shared high expression of monocyte and macrophage markers *Csf1r* and *Cd14* (**Figure S3A**). Of these eleven subpopulations, clusters 4, 5, 7, 8 and 10 had transcriptomic profiles representative of monocytes (**Figure 4A, C**). Clusters 4 was identified as *Ly6c2*$^{+}$ monocytes based on the robust expression of *Ly6c2* [49] and *Plac8* [50] (**Figure 4C, D**). Cluster 5 expressed high levels of

neutrophil markers S*100a8* and *S100a9*, in addition to *Ly6c2* and *Plac8* (**Figure 4A, C, Figure S3A-B**) and was named *S100a8*$^{+}$ monocytes. Cluster 8 cells displayed a unique expression profile. These cells showed low-moderate expression of monocyte markers such as *Ly6c2* and *Plac8*, as well as enrichment for neutrophil markers such as *S100a8* and *S100a9* and B cell markers such as *Cd79a* and *Igkc*. It has previously been reported that pre/pro-B cells can differentiate into macrophages [51] and this cluster was identified as *S100a8*$^{+}$*Cd79a*$^{+}$. Cluster 7 expressed both monocyte and macrophage markers as well as high levels of genes involved in interferon signaling (**Figure 4C-D, S1A-B**). This cluster was identified as interferon responsive Mono-Mac (*IfnR* Mono-Mac). Cluster 10 showed enrichment for genes such as *Cd300e*, *Ace* and *Fabp4*, in addition to moderate *Plac8* expression and was identified as *Cd300e*$^{+}$ (**Figure 4C, S3C**). When examining changes in various monocyte populations in response to injury, we observed a sharp increase in *Ly6c2*$^{+}$ and *S100a8*$^{+}$ monocytes immediately after injury, in both strains (**Figure 4D, Table S5**). Interestingly, B6 had a higher proportion of *Ly6c2*$^{+}$ monocytes relative to MRL at most timepoints examined while MRL had higher proportion of *S100a8*$^{+}$ monocytes (**Figure 4D, Table S5**).

Figure 4. Distinct gene expression profiles of monocyte and macrophage subpopulations. *(A) UMAP plot of monocyte and macrophage subpopulations identified from the parent Mono/Mac single cell cluster, colored by cell type. (B) UMAP plot of monocyte and macrophage subpopulations identified from the parent Mono/Mac single cell cluster, colored by experimental group. (C) Dot plots representing genes used to distinguish monocyte and macrophage subpopulations. (D) Feature plots of key monocyte and macrophage markers. (E) Changes of monocyte and macrophage subpopulations after injury from scRNA-seq data of B6 (solid line) and MRL (dashed line). The cell type proportions were calculated relative to all immune cells sequenced. Colors representative of clusters in Panel A.*

Cluster 6, monocyte-derived Dendritic Cells (MoDCs), were high in *Cd209a*, *Cd14* as well as MHC class II genes involved in antigen presentation such as *Cd74*, *H2-Ab1* and *H2-Aa* (**Figure 4C, S3A-B**). We also identified another small dendritic cell cluster (DC; cluster 9) which had high expression of MHC class II genes including *Cd74* and *H2-Ab1* and accounted for less than 2% of Mono/Macs at any timepoint examined (**Figure 4C, S3A-C**).

Clusters 1 and 3 expressed high levels of macrophage marker *Adgre1 (F4/80)* and the proportions of both clusters increased dramatically after injury in both strains (**Figure 4C-E**). Moreover, both subpopulations had high expression of *Trem2*, a gene that has been previously shown to promote myeloid cell phagocytosis [52-54], but *Trem2* was significantly enriched in cluster 1 (**Figure 4C, S3A-B**). Cluster 1 also showed enrichment for *Fcrls*, *Gas6*, *Apoe*, *C1qa* and *C1qb* and was named *Trem2*$^{+}$*Fcrls*$^{+}$. Cluster 2 highly expressed *Cav1* (Caveolin-1) (**Figure 4C**), a gene shown to promote monocyte to macrophage differentiation [55] as well as *Spp1*, *Vim*, *Arg1*, and *S100a4;* these macrophages were labeled *Spp1*$^{+}$*Cav1*$^{+}$. We also noted that clusters 1 and 2 were moderately comparable transcriptionally (**Figure S3B**) and clustered closely together in UMAP projections (**Figure 4A**). *Mrc1* (Cd206), a marker of alternatively activated macrophages, also known as M2 macrophages, was highly expressed in the *Trem2*$^{+}$*Fcrls*$^{+}$ cells, while the *Spp1*$^{+}$*Cav1*$^{+}$ population had very low expression (**Figure 4D, S3B**). The proportion of *Spp1*$^{+}$*Cav1*$^{+}$ population peaked at D1 in B6 while both *Trem2*$^{+}$*Fcrls*$^{+}$and *Spp1*$^{+}$*Cav1* macrophage populations peaked at D3 in MRL (**Figure 4E, Table S5**). Together these two macrophage subpopulations accounted for over 45% of all Mono/Macs at D3 in both strains (**Figure S3C**).

Cluster 2 had high expression of *Mrc1*, as well as several tissue resident macrophage markers including *Lyve1*, *Folr2*, *Vsig4 and Timd4* [56, 57]. This cluster was identified as *Lyve1*$^{+}$*Folr2*$^{+}$

macrophages. *Trem2* and its ligand *Apoe* were robustly expressed in this cluster (**Figure 4C, S3A-B**). MRLs had a significantly higher proportion of *Lyve1*$^{+}$*Folr2*$^{+}$ macrophages compared to B6 at nearly all timepoints examined (**Figure 4E**). Previously, our group identified that resident *Lyve1*^{high} macrophages localize primarily at the synovial lining within the uninjured knee joints of B6 mice in a highly organized fashion but infiltrate the synovium following injury and appear disorganized in the tissue (**Figure S4**) [28]. In this study, we also identified *Lyve1*$^{+}$ cells at the synovial lining of the MRL joint (**Figure S4**) but unlike B6, these cells remained highly organized post injury. *Lyve1*$^{+}$*Folr2*$^{+}$ macrophages expressed high levels of bone and cartilage anabolic growth factors, including *Bmp2* and *Igf1* (**Figure S3B**), suggesting that they may have a protective role in PTOA onset [27, 54, 58, 59] and may contribute to the resistance to PTOA seen in MRL joints.

Trem2^{+} macrophages have decreased inflammatory signaling in MRLs

While *Trem2*$^{+}$ *Fcrls*$^{+}$ and *Spp1*$^{+}$*Cav1*$^{+}$ subpopulations were essentially nonexistent in the uninjured joint, these populations displayed the largest shifts post injury in both strains (**Figure 4D**) suggesting that they are recruited to the joint tissue after injury. We observed *Ly6c2* expression in *Trem2*$^{+}$ *Fcrls*$^{+}$ and *Spp1*$^{+}$*Cav1*$^{+}$ macrophages at D1 (**Figure S4A**) as well as an increase in *Mrc1* expression primarily in *Trem2*$^{+}$ *Fcrls*$^{+}$ cells at D3-D7 suggesting that they are monocyte-derived, M2 polarized macrophages (**Figure 5A, Figure S4B**). This observation matched the population shifts observed in the *Ly6c*$^{+}$ Mono and *Trem2*$^{+}$ *Fcrls*$^{+}$ subpopulations **(Figure 4E**). However, it has been suggested that resident synovial macrophages may also polarize into *Trem2*$^{+}$ *Fcrls*$^{+}$ and *Spp1*$^{+}$*Cav1*$^{+}$ macrophage subpopulations [60]. To determine the differentiation trajectory of these recruited *Trem2*$^{+}$ macrophage subpopulations, we conducted a pseudo-time trajectory analysis with *Trem2*$^{+}$ *Fcrls*$^{+}$, *Spp1*$^{+}$*Cav1*$^{+}$, *IfnR*$^{+}$ and *Lyve1*$^{+}$ macrophages and *Ly6c2*$^{+}$ monocytes; *S100a8*$^{+}$ monocytes were excluded from this analysis as they appeared to be highly distant from *Trem2*$^{+}$

macrophages [28]. Pseudo-time analysis showed an expansion of *Ly6c2*$^+$ monocytes along the differentiation trajectory in the direction of *Trem2*$^+$ *Fcrls*$^+$ and *Spp1*$^+$*Cav1*$^+$ macrophages, primarily at D1 and D3 (**Figure 5A, S5**). Also, *Ly6c2* expression in these expanding cells coincided with the expression of *Trem2*, *Arg1*, a gene enriched in *Spp1*$^+$*Cav1*$^+$ specifically at D1 and D3, and macrophage marker *Adgre1* (F4/80) (**Figure 5, S5**). We observed an increase in *Mrc1* expression in these expanding cells primarily at D3, suggesting a monocytic origin for *Trem2*$^+$ *Fcrls*$^+$ and *Spp1*$^+$*Cav1*$^+$ macrophages (**Figure S5**). However, *Lyve1*$^+$ resident macrophages may also polarize into *Trem2*$^+$*Fcrls*$^+$ and *Spp1*$^+$*Cav1*$^+$ phenotype especially at later post-injury timepoints (**Figure 5, S5**).

Figure 5. Pseudo-time differentiation trajectory analysis of Trem2*$^+$*Fcrls*$^+$ *and Spp1*$^+$*Cav1*$^+$ *macrophages from MRL and B6. *(A) Pseudo-time trajectory analysis was conducted to determine potential origin of Trem2*$^+$*Fcrls*$^+$ *and Spp1*$^+$*Cav1*$^+$ *macrophages from Ly6c2*$^+$ *monocytes or tissue resident macrophages. The relative position of cells across the pseudo-time differentiation trajectory is depicted in the figure. Each point is a cell and is colored according to its cluster identity. For both MRL and B6, cells along the trajectory were divided into six groupings based on experimental timepoints (D0-4W). An expansion of Ly6c2*$^+$ *monocytes along the trajectory towards macrophages was observed after injury, primarily at D1 and D3 in both strains (indicated by arrows). B) Superimposition of the expression of monocyte marker Ly6c2 on the pseudo-time trajectory. Each point is a cell and is colored according to its pseudo-time value. Circle size represents the gene expression level. C) Superimposition of the expression of Arg1, a gene specifically enriched in Spp1*$^+$*Cav1*$^+$ *macrophages at D1-D3, on the pseudo-time trajectory. Expansion of cell populations expressing high levels of Arg1 in the monocyte to macrophage direction was observed after injury (indicated by arrows).*

To better understand transcriptomic changes in *Trem2*$^{+}$*Fcrls*$^{+}$ and *Spp1*$^{+}$*Cav1*$^{+}$ macrophages between strains and in response to injury, we performed differential expression analysis using Seurat (**Table S6**). Our analysis showed that *Trem2*$^{+}$*Fcrls*$^{+}$ and *Spp1*$^{+}$*Cav1*$^{+}$ macrophage subpopulations from B6 expressed significantly higher levels of genes associated with cytokine and pro-inflammatory signaling including *Ccl3, Ccl4, Ccl6, Ccl9, Il1b, Osm* and *Tnf* relative to MRL (**Figure 6A**). Gene ontology analysis of genes upregulated in B6 *Trem2*$^{+}$*Fcrls*$^{+}$ compared to MRL identified enrichment for biological processes such as 'leukocyte migration', 'cytokine production', 'inflammatory response', 'type II interferon production' and 'tumor necrosis factor production' (**Figure 6B**), indicating an enrichment of pro-inflammatory functions. These processes were also enriched in B6 *Spp1*$^{+}$*Cav1*$^{+}$ macrophages compared to MRL. In addition, *Spp1*$^{+}$*Cav1*$^{+}$ macrophages from B6 showed enrichment for genes associated with 'chronic inflammatory response', 'leukocyte proliferation' and 'regulation of interleukin-6 production' compared to MRL (**Figure 6B**).

Genes upregulated in MRL *Trem2*$^{+}$*Fcrls*$^{+}$ and *Spp1*$^{+}$*Cav1*$^{+}$ macrophages compared to B6 showed enrichment for processes such as 'wound healing', 'leukocyte activation', 'osteoclast differentiation', 'phagocytosis', 'mature B cell differentiation', 'response to oxidative stress', 'regulation of cell shape', 'membrane organization' and 'glutathione metabolic process' (**Figure 6B**). In addition, *Spp1*$^{+}$*Cav1*$^{+}$ macrophages from MRL showed enrichment for several lipid-associated processes including 'lipid transport', 'lipid storage' and 'lipid localization' (**Figure 6B**). Lipid transport or metabolism-associated genes enriched in MRL included *Cav1, Pltp, Trem2, Abcg1, Plin2, Aig1* and *Vps13c* **(Table S7).** We also identified multiple genes that were significantly higher (*Vwa5a* and *Glo1)* or exclusively (*Hal,* and *Ifi202b)* expressed in MRLs (**Figure 6A, C**). Many of these genes appeared to be differentially expressed between all MRL and B6 myeloid

subpopulations and these genes may represent inherent strain specific differences (**Figure 6A, C, S7A**).

Figure 6. Trem2 expressing macrophages have distinct transcriptional profiles and activation states in MRL and B6. *(A) Heatmap of a subset of genes differentially expressed in Trem2$^+$ Fcrls$^+$ and Spp1$^+$Cav1$^+$ macrophage populations from MRL and B6 joints (B) Enriched ontology terms associated with genes differentially expressed between MRL and B6 in Trem2$^+$ Fcrls$^+$ and Spp1$^+$Cav1$^+$ clusters. (C) Selected genes that are highly or exclusively expressed in MRL Trem2$^+$ Fcrls$^+$ and Spp1$^+$ Cav1$^+$ populations. (D) Pathways enriched in Trem2-expressing macrophage subpopulations.*

A pathway enrichment analysis revealed differential enrichment for several pathways between macrophage subpopulations and mouse strains (**Figure 6D**). *Trem2$^+$Fcrls$^+$* macrophages from B6 showed strong enrichment for TNF, NFKB, JAK/STAT and EGFR signaling compared to MRL, while MRL macrophages showed enrichment for VEGF signaling (**Figure 6D**). B6 *Spp1$^+$Cav1$^+$* macrophages showed enrichment for hypoxia pathway, MAPK, TNF, NFKB, EGFR, PI3K and JAK/STAT signaling compared to MRL (**Figure 6D**). We also observed that, in both strains, TNF, NFKB, JAK/STAT and EGFR signaling was enriched in *Trem2$^+$ Fcrls$^+$* macrophages relative to *Spp1$^+$Cav1$^+$* macrophages while *Spp1$^+$Cav1$^+$* macrophages showed enrichment for hypoxia, MAPK and VEGF signaling (**Figure 6D**). Consistent with this, a transcription factor binding motif analysis identified hypoxia transcription factors *Hif1a* and *Hif2a* (Epas1) as enriched in *Spp1$^+$Cav1$^+$* macrophages, with the highest enrichment in B6 mice (**Figure S7B**). *Hif1α* gene expression was also enriched in *Spp1$^+$Cav1$^+$* macrophages along with multiple genes encoding for glycolytic enzymes such as *Ldha* and *Eno1*, potentially regulated by Hif1α [61, 62] (**Figure S7C**). In addition to *Mrc1*, *Trem2$^+$Fcrls$^+$* macrophages showed strong enrichment for several other genes

519 highly expressed in M2 macrophages such as *Il10*, *Marcks* and *Cd83*, which were also shared by
520 *Lyve1*$^{+}$*Folr2*$^{+}$ resident macrophages (**Figure S7C, S3B**).

521 **Sustained Trem2^{+} M2 macrophage populations in MRLs may promote tissue repair**

522 To further identify trends in macrophage infiltration and M2 activation that may contribute to
523 MRL's resilience to PTOA development, *Mrc1*- and *Trem2*– expressing macrophage subpopulations
524 from scRNA-seq data were compared between B6 and MRL across all timepoints (**Figure 7A**).
525 Uninjured MRL joints had a higher proportion of *Mrc1*$^{+}$ cells than B6 and sustained a consistently
526 higher proportion at all timepoints indicating an increase in macrophage polarize towards an M2
527 phenotype in this strain (**Figure 7A**). The majority of *Mrc1*$^{+}$ cells also expressed high levels of
528 *Trem2* in both strains (**Figure 7A, S3B**). The increased levels of *Mrc1*$^{+}$*Trem2*$^{+}$ cells in the MRL
529 joints suggest that M2 macrophages expressing *Trem2* may play a vital role in injury response and
530 promote the enhanced healing associated with this strain.
531
532 ***Figure 7. Flow cytometry and immunohistochemistry analysis confirm an increased presence of***
533 ***CD206^{+}Trem2^{+} macrophages in MRL knee joints.*** *A) Proportion of Mrc1*$^{+}$ *and Mrc1*$^{+}$*Trem2*$^{+}$
534 *Mono/Macs relative to total immune cells sequenced in both B6 (solid red line) and MRL (dotted*
535 *blue line) across all injury timepoints. (B) Representative gating scheme for the analysis of*
536 *macrophages (CD45*$^{+}$*F4/80*$^{+}$*) that have shifts in CD206 and Trem2 expression between strains*
537 *within digested synovial joint immune populations at D7. (C) Proportion of cells in B6 and MRL*
538 *with macrophage expression profiles of CD45*$^{+}$*F4/80*$^{+}$*CD206*$^{+}$*Trem2*$^{+}$*, n=5; **p<0.01,*
539 ****p<0.001, ****p<0.0001, n=3-5 / group. (D) Immunohistochemistry evaluation of macrophages*
540 *expressing Trem2 in MRL and B6 at D0 (uninjured), D7 post injury and 4W post injury. n=5 /*
541 *group. Scale Bars = 200µm, 20x Magnification, Red – CD206, Green – Trem2, Blue – Nuclei.*

Further validation of *Mrc1* (CD206) and *Trem2* expression was conducted by flow cytometry (**Figure 7B-C**). Viable $CD45^+F4/80^+$ cells were gated as the macrophage population and then analyzed for shifts in CD206 (Mrc1) and Trem2 protein expression in uninjured and D7 post injury joints (**Figure 7B-C**). Consistent with the scRNA-seq data, we observed a large spike in the $CD206^+Trem2^+$ population at D7 in both strains. In addition, MRLs had significantly more $CD206^+Trem2^+$ macrophages than B6 at D7 post injury (**Figure 7C**). Shifts in $CD206^+Trem2^+$ macrophages were also validated at the protein level through immunofluorescence of synovial joints (**Figure 7D**). In uninjured joints, MRL had a stronger Trem2 expression than B6 (**Figure 7D;** D0), and robust expression of CD206 was seen throughout the synovium of the knee joint compared to B6. At D7, $CD206^+Trem2^+$ expression was higher in MRL joints than B6 as indicated by the yellow co-expression of Trem2 and CD206 (**Figure 7D**).

Discussion

This study sheds new light on the important modulatory role immune cells have in the prevention or onset of chronic joint degeneration. scRNA-seq and a non-surgical injury method allowed the unbiased examination of the immune heterogeneity in the synovial knee joint of PTOA-susceptible B6 mice and PTOA-resistant MRL mice [28, 45, 63, 64]. Previous studies have implicated infiltrating myeloid-derived populations, such as neutrophils and monocytes, as culprits of a pro-inflammatory joint state during osteoarthritis progression [1, 65, 66]. These cells are responsible for the production of inflammatory cytokines and chemokines, such as *IL-1β, TNFα, IL-6, IL-10,* and *IL-15*, as well as many others from the CCL/CXCL family [66]. Many of these molecular signals may be responsible for the infiltration of innate (macrophages, neutrophils, NK) and adaptive (T, B) immune cells into the synovial joint. Here, we characterized resident and infiltrating monocyte and macrophage subpopulations as well as neutrophils present in the synovial knee joint of MRL and B6

mice. Previously, *Ly6c*^{high} monocytes have been shown to be recruited to the joint in response to traumatic knee injury and act as pro-inflammatory effector cells in tissues with perturbed homeostasis [67]. We found B6 joints to consistently have higher numbers of *Ly6c*$^{+}$ monocytes than MRL while the MRLs had an increased number of M2 macrophages.

A major M2-like macrophage population identified in the synovial joint was the resident *Lyve1*$^{+}$ macrophages. In addition to established tissue resident macrophage markers such as *Lyve1*, *Folr2* and *Vsig4*, *Lyve1*+ macrophages expressed *Trem2*, its ligand *Apoe* and several growth factors with potential chondroprotective functions such as *Igf1* and *Bmp2* [68, 69]. *Trem2* expression has previously been associated with macrophages responsible for forming a protective barrier in synovial joints [21, 28]. *Trem2*$^{+}$ alternatively activated macrophages have been shown to drive an anti-inflammatory tissue environment and to promote damage repair *via* stromal cell interactions in RA joints as well as in other tissues [70, 71], therefore the increase in the *Trem2*$^{+}$ M2-like macrophage population after an injury is likely to confer a protective phenotype. Although the proportion of *Lyve1*$^{+}$ macrophages did not change considerably over time, MRL constantly had more *Lyve1*$^{+}$ macrophages than B6 at all timepoints. We also found that *Lyve1*$^{+}$ macrophages from B6 expressed higher levels of inflammatory cytokines (*Tnf*, *Ccl3*, *Ccl4*) than MRL, suggesting that *Lyve1*$^{+}$ macrophages in B6 are likely proinflammatory.

In addition to resident *Lyve1*$^{+}$ macrophages, *Trem2* was also expressed in *Trem2*$^{+}$*Fcrls*$^{+}$ and *Spp1*$^{+}$*Cav1*$^{+}$ macrophage clusters, with significantly higher expression in *Trem2*$^{+}$*Fcrls*$^{+}$ cluster than *Spp1*$^{+}$*Cav1*$^{+}$ cluster. Starting at D1 post injury, MRL and B6 synovium experienced an increase in the proportion of both *Trem2*$^{+}$*Fcrls*$^{+}$ and *Spp1*$^{+}$*Cav1*$^{+}$ macrophages. Both these clusters expressed low levels of *Ly6c2* at D1 indicating these cells were monocyte derived and emerged into the synovial joints after injury. Further gene and ontology enrichment analysis of *Trem2*$^{+}$ recruited

588 macrophages identified a more pro-inflammatory molecular phenotype in B6 cells. Specifically,
589 *Trem2*$^{+}$ infiltrating macrophages in B6 were highly associated with proinflammatory cytokine
590 expression and ontologies associated with inflammatory response. In contrast, several genes highly
591 expressed in MRLs were associated with biological processes such as wound healing and response to
592 oxidative stress.

593 *Trem2*$^{+}$*Fcrls*$^{+}$ macrophages also expressed high levels of M2 marker *Mrc1* (CD206) and
594 several other genes enriched in M2 macrophages including *Cd83, Marcks* and *Apoe* suggesting that
595 this population shares some similar functions with the *Lyve1*$^{+}$ population. Flow cytometry analysis
596 confirmed that MRL has significantly more *CD206*$^{+}$*Trem2*$^{+}$macrophages than B6 at D7. The
597 sustained level of *Trem2*$^{+}$ macrophages in MRLs suggests that MRLs are better equipped to respond
598 to injury through recruitment of hematopoietic progenitors and M2 polarization *via* cytokine
599 signaling, such that phagocytosis of apoptotic cells induced by initial joint inflammation is more
600 effective and promotes healing [72, 73].

601 *Spp1*$^{+}$*Cav1*$^{+}$ macrophages shared molecular signatures (*Spp1, Fn1, Arg1, Capg* etc.) with
602 previously described *Spp1*$^{+}$ pro-fibrotic macrophages [74]. In line with the findings by Hoeft *et al*,
603 *Spp1*$^{+}$ macrophages showed strong enrichment for Hypoxia-inducible factor 1α (*Hif1α*) signaling
604 [74]. *Hif1α* promotes the switch from oxidative phosphorylation to glycolysis so that cells can
605 continue to produce ATP when oxygen is limited, as oxygen is not required for glycolysis [75].
606 Consistent with *Hif1α* activation, we observed an increase in the expression of glycolytic enzymes
607 including *Ldha, Eno1* and *Aldoa* in *Spp1*$^{+}$*Cav1*$^{+}$ macrophages, all of which had higher expression in
608 MRL compared to B6. Further studies are required to understand if increased expression of these
609 glycolytic enzymes helps with the enhanced healing or PTOA resistance observed in MRL. Knight

610 *et al* suggested that these pro-fibrotic macrophages arise from synovial resident macrophages after
611 injury [60]. However, our monocle trajectory analysis suggested that *Ly6c2*$^{+}$ monocytes could also
612 differentiate into *Spp1*$^{+}$ macrophages especially at early post-injury timepoints, which is consistent
613 with the findings by Ramachandran *et al*, in liver cirrhosis [76]. Thorough *in vivo* fate mapping
614 studies are required to elucidate the true origins of these cells.

615 We also identified several genes consistently upregulated in all monocytes and macrophages
616 from MRL, many of which had the highest expression in *Trem2*+ macrophages. Specifically, *Glo1*
617 has been shown to help inhibit inflammation by managing methylglyoxal levels produced by
618 macrophages, thus inhibiting cell death and cytokine production [77]. An increase in *Glo1*
619 expression in *Trem2*$^{+}$ macrophages from MRL indicates that these cells may play an essential role in
620 dampening proinflammatory signaling in MRL most likely through reactive oxygen compounds or
621 metabolites by locally damaged cells.

622 Neutrophils were a major immune population identified in our data. Although we failed to
623 detect a considerable number of neutrophils in the knee joint tissues *via* IHC, we were able to rule
624 out contamination from the circulation or the BM as possible origins of these neutrophils. This
625 suggests that these neutrophils likely reside within the joint or adjacent tissues such as fat pad or the
626 bone. Neutrophils expressed high levels of inflammatory cytokines (*Il1b*, *Tnf*, *Osm* etc.) and matrix
627 degrading enzymes (*Mmp8*, *Mmp9* etc.) in both MRL and B6. We also noted that MRL neutrophils
628 had lower expression of *Il1β* compared to B6 but, had higher expression of endogenous Il1 receptor
629 antagonist *Il1rn*. In addition, MRL neutrophils expressed higher levels of *Csf1*, a key growth factor
630 required for macrophage differentiation [78], than B6, which may have contributed to the increased
631 presence of macrophages in MRL joints. This indicates that the presence of neutrophils in the joint

may contribute to differences in injury outcomes observed in MRL and B6. Our data highlights gene expression changes in response to injury and strain specific differences in neutrophils. However, further studies are needed to localize neutrophils in the articular joint forming tissues and understand their specific role in PTOA pathogenesis.

Conclusions

This study represents the first report describing fundamental molecular and cellular differences in neutrophil and macrophage subpopulations and macrophage polarization in the injured joint that may set the super-healer MRL strain apart from B6. The significant enrichment and sustained high levels of tissue-resident *CD206*$^{+}$*Trem2*$^{+}$ macrophages in this strain may be an essential characteristic for successful cartilage tissue remodeling, macrophage turnover, and joint protection during early injury responses, preventing transition to the chronic phase of PTOA. Further exploration of these polarized macrophages in patients and animal models will help us determine why some individuals fully recover from an ACL injury without developing PTOA, while others succumb to this degenerative disorder.

ACKNOWLEDGEMENTS

This work was performed under the auspices of the U.S. Department of Energy by Lawrence Livermore National Laboratory under Contract DE-AC52-07NA27344. JLM, AS, NRH, DKM and SPW were supported by Lawrence Livermore National Laboratory LDRD 20-LW-002. AS, DKM, NRH, SPW, BA and GGL were supported by Department of Defense Awards PR180268 and PR192271. BAC was supported by the National Institute of Health grant R01 AR075013 and Department of Defense Award PR180268P1.

Author's Role: Study design: JLM, AS and GGL; Data acquisition: JLM, DKM, CM, NRH, BA, and BAC. Data analysis and interpretation: JLM, AS, OAD, SPW, BAC, and GGL. JLM, AS and GGL wrote the manuscript.

Data Availability Statement. The datasets generated for this study can be found in the Gene Expression Omnibus (GEO) under accession numbers GSE200843 and GSE220167.

REFERENCES

1. Punzi L, Galozzi P, Luisetto R, Favero M, Ramonda R, Oliviero F, et al. Post-traumatic arthritis: overview on pathogenic mechanisms and role of inflammation. RMD Open. 2016;2(2):e000279. Epub 20160906. doi: 10.1136/rmdopen-2016-000279. PubMed PMID: 27651925; PubMed Central PMCID: PMCPMC5013366.

2. Heydemann A. The super super-healing MRL mouse strain. Front Biol (Beijing). 2012;7(6):522-38. doi: 10.1007/s11515-012-1192-4. PubMed PMID: 24163690; PubMed Central PMCID: PMCPMC3806350.

3. Fitzgerald J, Rich C, Burkhardt D, Allen J, Herzka AS, Little CB. Evidence for articular cartilage regeneration in MRL/MpJ mice. Osteoarthritis Cartilage. 2008;16(11):1319-26. Epub 20080501. doi: 10.1016/j.joca.2008.03.014. PubMed PMID: 18455447.

4. Clark LD, Clark RK, Heber-Katz E. A new murine model for mammalian wound repair and regeneration. Clin Immunol Immunopathol. 1998;88(1):35-45. doi: 10.1006/clin.1998.4519. PubMed PMID: 9683548.

5. Kwiatkowski A, Piatkowski M, Chen M, Kan L, Meng Q, Fan H, et al. Superior angiogenesis facilitates digit regrowth in MRL/MpJ mice compared to C57BL/6 mice. Biochem Biophys Res Commun. 2016;473(4):907-12. Epub 20160331. doi: 10.1016/j.bbrc.2016.03.149. PubMed PMID: 27040769.

6. Mendez ME, Sebastian A, Murugesh DK, Hum NR, McCool JL, Hsia AW, et al. LPS-Induced Inflammation Prior to Injury Exacerbates the Development of Post-Traumatic Osteoarthritis in Mice. J Bone Miner Res. 2020;35(11):2229-41. Epub 20200803. doi: 10.1002/jbmr.4117. PubMed PMID: 32564401; PubMed Central PMCID: PMCPMC7689775.

7. Rai MF, Sandell LJ. Regeneration of articular cartilage in healer and non-healer mice. Matrix Biol. 2014;39:50-5. Epub 20140828. doi: 10.1016/j.matbio.2014.08.011. PubMed PMID: 25173437; PubMed Central PMCID: PMCPMC4306343.

8. Rajnoch C, Ferguson S, Metcalfe AD, Herrick SE, Willis HS, Ferguson MW. Regeneration of the ear after wounding in different mouse strains is dependent on the severity of wound trauma. Dev Dyn. 2003;226(2):388-97. doi: 10.1002/dvdy.10242. PubMed PMID: 12557217.

9. Sebastian A, Chang JC, Mendez ME, Murugesh DK, Hatsell S, Economides AN, et al. Comparative Transcriptomics Identifies Novel Genes and Pathways Involved in Post-Traumatic Osteoarthritis Development and Progression. Int J Mol Sci. 2018;19(9). Epub 20180907. doi: 10.3390/ijms19092657. PubMed PMID: 30205482; PubMed Central PMCID: PMCPMC6163882.

10. Ward BD, Furman BD, Huebner JL, Kraus VB, Guilak F, Olson SA. Absence of posttraumatic arthritis following intraarticular fracture in the MRL/MpJ mouse. Arthritis Rheum. 2008;58(3):744-53. doi: 10.1002/art.23288. PubMed PMID: 18311808.

11. Khella CM, Horvath JM, Asgarian R, Rolauffs B, Hart ML. Anti-Inflammatory Therapeutic Approaches to Prevent or Delay Post-Traumatic Osteoarthritis (PTOA) of the Knee Joint with a Focus on Sustained Delivery Approaches. Int J Mol Sci. 2021;22(15). Epub 20210727. doi: 10.3390/ijms22158005. PubMed PMID: 34360771; PubMed Central PMCID: PMCPMC8347094.

12. Anderson DD, Chubinskaya S, Guilak F, Martin JA, Oegema TR, Olson SA, et al. Post-traumatic osteoarthritis: improved understanding and opportunities for early intervention. J Orthop

699 Res. 2011;29(6):802-9. Epub 20110211. doi: 10.1002/jor.21359. PubMed PMID: 21520254;
700 PubMed Central PMCID: PMCPMC3082940.
701 13. Dymock DC, Brown MP, Merritt KA, Trumble TN. Concentrations of stromal cell-derived
702 factor-1 in serum, plasma, and synovial fluid of horses with osteochondral injury. Am J Vet Res.
703 2014;75(8):722-30. doi: 10.2460/ajvr.75.8.722. PubMed PMID: 25061703.
704 14. El-Hadi M, Charavaryamath C, Aebischer A, Smith CW, Shmon C, Singh B. Expression of
705 interleukin-8 and intercellular cell adhesion molecule-1 in the synovial membrane and cranial
706 cruciate ligament of dogs after rupture of the ligament. Can J Vet Res. 2012;76(1):8-15. PubMed
707 PMID: 22754089; PubMed Central PMCID: PMCPMC3244294.
708 15. Ferrándiz ML, Terencio MC, Ruhí R, Vergés J, Montell E, Torrent A, et al. Influence of age
709 on osteoarthritis progression after anterior cruciate ligament transection in rats. Exp Gerontol.
710 2014;55:44-8. Epub 20140322. doi: 10.1016/j.exger.2014.03.010. PubMed PMID: 24667123.
711 16. Shen PC, Lu CS, Shiau AL, Lee CH, Jou IM, Hsieh JL. Lentiviral small hairpin RNA
712 knockdown of macrophage inflammatory protein-1γ ameliorates experimentally induced
713 osteoarthritis in mice. Hum Gene Ther. 2013;24(10):871-82. doi: 10.1089/hum.2012.189. PubMed
714 PMID: 24016310; PubMed Central PMCID: PMCPMC3787402.
715 17. Loeser RF, Olex AL, McNulty MA, Carlson CS, Callahan M, Ferguson C, et al. Disease
716 progression and phasic changes in gene expression in a mouse model of osteoarthritis. PLoS One.
717 2013;8(1):e54633. Epub 20130128. doi: 10.1371/journal.pone.0054633. PubMed PMID: 23382930;
718 PubMed Central PMCID: PMCPMC3557277.
719 18. Khella CM, Asgarian R, Horvath JM, Rolauffs B, Hart ML. An Evidence-Based Systematic
720 Review of Human Knee Post-Traumatic Osteoarthritis (PTOA): Timeline of Clinical Presentation
721 and Disease Markers, Comparison of Knee Joint PTOA Models and Early Disease Implications. Int J

Mol Sci. 2021;22(4). Epub 20210217. doi: 10.3390/ijms22041996. PubMed PMID: 33671471; PubMed Central PMCID: PMCPMC7922905.

19. Kim-Wang SY, Holt AG, McGowan AM, Danyluk ST, Goode AP, Lau BC, et al. Immune cell profiles in synovial fluid after anterior cruciate ligament and meniscus injuries. Arthritis Res Ther. 2021;23(1):280. Epub 20211104. doi: 10.1186/s13075-021-02661-1. PubMed PMID: 34736523; PubMed Central PMCID: PMCPMC8567695.

20. Haseeb A, Haqqi TM. Immunopathogenesis of osteoarthritis. Clin Immunol. 2013;146(3):185-96. Epub 20130106. doi: 10.1016/j.clim.2012.12.011. PubMed PMID: 23360836; PubMed Central PMCID: PMCPMC4015466.

21. Culemann S, Grüneboom A, Nicolás-Ávila J, Weidner D, Lämmle KF, Rothe T, et al. Locally renewing resident synovial macrophages provide a protective barrier for the joint. Nature. 2019;572(7771):670-5. Epub 20190807. doi: 10.1038/s41586-019-1471-1. PubMed PMID: 31391580; PubMed Central PMCID: PMCPMC6805223.

22. Croft AP, Campos J, Jansen K, Turner JD, Marshall J, Attar M, et al. Distinct fibroblast subsets drive inflammation and damage in arthritis. Nature. 2019;570(7760):246-51. Epub 20190529. doi: 10.1038/s41586-019-1263-7. PubMed PMID: 31142839; PubMed Central PMCID: PMCPMC6690841.

23. Orr C, Vieira-Sousa E, Boyle DL, Buch MH, Buckley CD, Cañete JD, et al. Synovial tissue research: a state-of-the-art review. Nat Rev Rheumatol. 2017;13(8):463-75. Epub 20170713. doi: 10.1038/nrrheum.2017.115. PubMed PMID: 28701760.

24. Knab K, Chambers D, Krönke G. Synovial Macrophage and Fibroblast Heterogeneity in Joint Homeostasis and Inflammation. Front Med (Lausanne). 2022;9:862161. Epub 20220425. doi:

10.3389/fmed.2022.862161. PubMed PMID: 35547214; PubMed Central PMCID: PMCPMC9081642.

25. Fujiwara N, Kobayashi K. Macrophages in inflammation. Curr Drug Targets Inflamm Allergy. 2005;4(3):281-6. doi: 10.2174/1568010054022024. PubMed PMID: 16101534.

26. Lech M, Anders HJ. Macrophages and fibrosis: How resident and infiltrating mononuclear phagocytes orchestrate all phases of tissue injury and repair. Biochim Biophys Acta. 2013;1832(7):989-97. Epub 20121213. doi: 10.1016/j.bbadis.2012.12.001. PubMed PMID: 23246690.

27. Mescher AL. Macrophages and fibroblasts during inflammation and tissue repair in models of organ regeneration. Regeneration (Oxf). 2017;4(2):39-53. Epub 20170606. doi: 10.1002/reg2.77. PubMed PMID: 28616244; PubMed Central PMCID: PMCPMC5469729.

28. Sebastian A, Hum NR, McCool JL, Wilson SP, Murugesh DK, Martin KA, et al. Single-cell RNA-Seq reveals changes in immune landscape in post-traumatic osteoarthritis. Front Immunol. 2022;13:938075. Epub 20220729. doi: 10.3389/fimmu.2022.938075. PubMed PMID: 35967299; PubMed Central PMCID: PMCPMC9373730.

29. Christiansen BA, Anderson MJ, Lee CA, Williams JC, Yik JH, Haudenschild DR. Musculoskeletal changes following non-invasive knee injury using a novel mouse model of post-traumatic osteoarthritis. Osteoarthritis Cartilage. 2012;20(7):773-82. Epub 20120421. doi: 10.1016/j.joca.2012.04.014. PubMed PMID: 22531459.

30. Liu H, Zhu R, Liu C, Ma R, Wang L, Chen B, et al. Evaluation of Decalcification Techniques for Rat Femurs Using HE and Immunohistochemical Staining. Biomed Res Int. 2017;2017:9050754. Epub 20170126. doi: 10.1155/2017/9050754. PubMed PMID: 28246608; PubMed Central PMCID: PMCPMC5299168.

31. Schneider CA, Rasband WS, Eliceiri KW. NIH Image to ImageJ: 25 years of image analysis. Nat Methods. 2012;9(7):671-5. doi: 10.1038/nmeth.2089. PubMed PMID: 22930834; PubMed Central PMCID: PMCPMC5554542.

32. Glasson SS, Chambers MG, Van Den Berg WB, Little CB. The OARSI histopathology initiative - recommendations for histological assessments of osteoarthritis in the mouse. Osteoarthritis Cartilage. 2010;18 Suppl 3:S17-23. doi: 10.1016/j.joca.2010.05.025. PubMed PMID: 20864019.

33. Hao Y, Hao S, Andersen-Nissen E, Mauck WM, 3rd, Zheng S, Butler A, et al. Integrated analysis of multimodal single-cell data. Cell. 2021;184(13):3573-87 e29. Epub 20210531. doi: 10.1016/j.cell.2021.04.048. PubMed PMID: 34062119; PubMed Central PMCID: PMCPMC8238499.

34. Korsunsky I, Millard N, Fan J, Slowikowski K, Zhang F, Wei K, et al. Fast, sensitive and accurate integration of single-cell data with Harmony. Nat Methods. 2019;16(12):1289-96. Epub 20191118. doi: 10.1038/s41592-019-0619-0. PubMed PMID: 31740819; PubMed Central PMCID: PMCPMC6884693.

35. Wu T, Hu E, Xu S, Chen M, Guo P, Dai Z, et al. clusterProfiler 4.0: A universal enrichment tool for interpreting omics data. Innovation (Camb). 2021;2(3):100141. Epub 20210701. doi: 10.1016/j.xinn.2021.100141. PubMed PMID: 34557778; PubMed Central PMCID: PMCPMC8454663.

36. Alexa A, Rahnenfuhrer J, Lengauer T. Improved scoring of functional groups from gene expression data by decorrelating GO graph structure. Bioinformatics. 2006;22(13):1600-7. Epub 20060410. doi: 10.1093/bioinformatics/btl140. PubMed PMID: 16606683.

37. Chen J, Bardes EE, Aronow BJ, Jegga AG. ToppGene Suite for gene list enrichment analysis and candidate gene prioritization. Nucleic Acids Res. 2009;37(Web Server issue):W305-11. Epub 20090522. doi: 10.1093/nar/gkp427. PubMed PMID: 19465376; PubMed Central PMCID: PMCPMC2703978.

38. Badia IMP, Velez Santiago J, Braunger J, Geiss C, Dimitrov D, Muller-Dott S, et al. decoupleR: ensemble of computational methods to infer biological activities from omics data. Bioinform Adv. 2022;2(1):vbac016. Epub 20220308. doi: 10.1093/bioadv/vbac016. PubMed PMID: 36699385; PubMed Central PMCID: PMCPMC9710656.

39. Blanco-Carmona E. Generating publication ready visualizations for Single Cell transcriptomics using SCpubr. bioRxiv. 2022:2022.02.28.482303. doi: 10.1101/2022.02.28.482303.

40. Frerebeau N. khroma: Colour Schemes for Scientific Data Visualization2024.

41. Wickham H, Averick M, Bryan J, Chang W, McGowan LDA, François R, et al. Welcome to the Tidyverse. Journal of Open Source Software. 2019;4(43):1686. doi: 10.21105/joss.01686.

42. Qiu X, Mao Q, Tang Y, Wang L, Chawla R, Pliner HA, et al. Reversed graph embedding resolves complex single-cell trajectories. Nat Methods. 2017;14(10):979-82. Epub 20170821. doi: 10.1038/nmeth.4402. PubMed PMID: 28825705; PubMed Central PMCID: PMCPMC5764547.

43. Blaker CL, Clarke EC, Little CB. Using mouse models to investigate the pathophysiology, treatment, and prevention of post-traumatic osteoarthritis. J Orthop Res. 2017;35(3):424-39. Epub 20160628. doi: 10.1002/jor.23343. PubMed PMID: 27312470.

44. Chang JC, Sebastian A, Murugesh DK, Hatsell S, Economides AN, Christiansen BA, et al. Global molecular changes in a tibial compression induced ACL rupture model of post-traumatic osteoarthritis. J Orthop Res. 2017;35(3):474-85. Epub 20160510. doi: 10.1002/jor.23263. PubMed PMID: 27088242; PubMed Central PMCID: PMCPMC5363336.

45. Sebastian A, McCool JL, Hum NR, Murugesh DK, Wilson SP, Christiansen BA, et al. Single-Cell RNA-Seq Reveals Transcriptomic Heterogeneity and Post-Traumatic Osteoarthritis-Associated Early Molecular Changes in Mouse Articular Chondrocytes. Cells. 2021;10(6). Epub 20210610. doi: 10.3390/cells10061462. PubMed PMID: 34200880; PubMed Central PMCID: PMCPMC8230441.

46. Garley M, Jablonska E. Heterogeneity Among Neutrophils. Arch Immunol Ther Exp (Warsz). 2018;66(1):21-30. Epub 20170530. doi: 10.1007/s00005-017-0476-4. PubMed PMID: 28560557; PubMed Central PMCID: PMCPMC5767199.

47. Grieshaber-Bouyer R, Radtke FA, Cunin P, Stifano G, Levescot A, Vijaykumar B, et al. The neutrotime transcriptional signature defines a single continuum of neutrophils across biological compartments. Nat Commun. 2021;12(1):2856. Epub 20210517. doi: 10.1038/s41467-021-22973-9. PubMed PMID: 34001893; PubMed Central PMCID: PMCPMC8129206.

48. Villatoro A, Cuminetti V, Bernal A, Torroja C, Cossio I, Benguria A, et al. Author Correction: Endogenous IL-1 receptor antagonist restricts healthy and malignant myeloproliferation. Nat Commun. 2023;14(1):3874. Epub 20230630. doi: 10.1038/s41467-023-39601-3. PubMed PMID: 37391415; PubMed Central PMCID: PMCPMC10313788.

49. Menezes S, Melandri D, Anselmi G, Perchet T, Loschko J, Dubrot J, et al. The Heterogeneity of Ly6C(hi) Monocytes Controls Their Differentiation into iNOS(+) Macrophages or Monocyte-Derived Dendritic Cells. Immunity. 2016;45(6):1205-18. doi: 10.1016/j.immuni.2016.12.001. PubMed PMID: 28002729; PubMed Central PMCID: PMCPMC5196026.

50. Kemp SB, Steele NG, Carpenter ES, Donahue KL, Bushnell GG, Morris AH, et al. Pancreatic cancer is marked by complement-high blood monocytes and tumor-associated

macrophages. Life Sci Alliance. 2021;4(6). Epub 20210329. doi: 10.26508/lsa.202000935. PubMed PMID: 33782087; PubMed Central PMCID: PMCPMC8091600.

51. Audzevich T, Bashford-Rogers R, Mabbott NA, Frampton D, Freeman TC, Potocnik A, et al. Pre/pro-B cells generate macrophage populations during homeostasis and inflammation. Proc Natl Acad Sci U S A. 2017;114(20):E3954-E63. Epub 20170501. doi: 10.1073/pnas.1616417114. PubMed PMID: 28461481; PubMed Central PMCID: PMCPMC5441795.

52. Zhong L, Chen XF, Wang T, Wang Z, Liao C, Wang Z, et al. Soluble TREM2 induces inflammatory responses and enhances microglial survival. J Exp Med. 2017;214(3):597-607. Epub 20170216. doi: 10.1084/jem.20160844. PubMed PMID: 28209725; PubMed Central PMCID: PMCPMC5339672.

53. Kobayashi M, Konishi H, Sayo A, Takai T, Kiyama H. TREM2/DAP12 Signal Elicits Proinflammatory Response in Microglia and Exacerbates Neuropathic Pain. J Neurosci. 2016;36(43):11138-50. doi: 10.1523/jneurosci.1238-16.2016. PubMed PMID: 27798193; PubMed Central PMCID: PMCPMC6705657.

54. Alivernini S, MacDonald L, Elmesmari A, Finlay S, Tolusso B, Gigante MR, et al. Distinct synovial tissue macrophage subsets regulate inflammation and remission in rheumatoid arthritis. Nat Med. 2020;26(8):1295-306. Epub 20200629. doi: 10.1038/s41591-020-0939-8. PubMed PMID: 32601335.

55. Fu Y, Moore XL, Lee MK, Fernández-Rojo MA, Parat MO, Parton RG, et al. Caveolin-1 plays a critical role in the differentiation of monocytes into macrophages. Arterioscler Thromb Vasc Biol. 2012;32(9):e117-25. Epub 20120705. doi: 10.1161/atvbaha.112.254151. PubMed PMID: 22772753.

56. Zernecke A, Erhard F, Weinberger T, Schulz C, Ley K, Saliba AE, et al. Integrated single-cell analysis-based classification of vascular mononuclear phagocytes in mouse and human atherosclerosis. Cardiovasc Res. 2023;119(8):1676-89. doi: 10.1093/cvr/cvac161. PubMed PMID: 36190844; PubMed Central PMCID: PMCPMC10325698.

57. Dick SA, Wong A, Hamidzada H, Nejat S, Nechanitzky R, Vohra S, et al. Three tissue resident macrophage subsets coexist across organs with conserved origins and life cycles. Sci Immunol. 2022;7(67):eabf7777. Epub 20220107. doi: 10.1126/sciimmunol.abf7777. PubMed PMID: 34995099.

58. Chakarov S, Lim HY, Tan L, Lim SY, See P, Lum J, et al. Two distinct interstitial macrophage populations coexist across tissues in specific subtissular niches. Science. 2019;363(6432). doi: 10.1126/science.aau0964. PubMed PMID: 30872492.

59. Dick SA, Macklin JA, Nejat S, Momen A, Clemente-Casares X, Althagafi MG, et al. Self-renewing resident cardiac macrophages limit adverse remodeling following myocardial infarction. Nat Immunol. 2019;20(1):29-39. Epub 20181211. doi: 10.1038/s41590-018-0272-2. PubMed PMID: 30538339; PubMed Central PMCID: PMCPMC6565365.

60. Knights AJ, Farrell EC, Ellis OM, Song MJ, Appleton CT, Maerz T. Synovial macrophage diversity and activation of M-CSF signaling in post-traumatic osteoarthritis. bioRxiv. 2023. Epub 20231005. doi: 10.1101/2023.10.03.559514. PubMed PMID: 37873464; PubMed Central PMCID: PMCPMC10592932.

61. Cui XG, Han ZT, He SH, Wu XD, Chen TR, Shao CH, et al. HIF1/2alpha mediates hypoxia-induced LDHA expression in human pancreatic cancer cells. Oncotarget. 2017;8(15):24840-52. doi: 10.18632/oncotarget.15266. PubMed PMID: 28193910; PubMed Central PMCID: PMCPMC5421893.

62. Zheng F, Jang WC, Fung FK, Lo AC, Wong IY. Up-Regulation of ENO1 by HIF-1alpha in Retinal Pigment Epithelial Cells after Hypoxic Challenge Is Not Involved in the Regulation of VEGF Secretion. PLoS One. 2016;11(2):e0147961. Epub 20160216. doi: 10.1371/journal.pone.0147961. PubMed PMID: 26882120; PubMed Central PMCID: PMCPMC4755565.

63. Li X, Liao Z, Deng Z, Chen N, Zhao L. Combining bulk and single-cell RNA-sequencing data to reveal gene expression pattern of chondrocytes in the osteoarthritic knee. Bioengineered. 2021;12(1):997-1007. doi: 10.1080/21655979.2021.1903207. PubMed PMID: 33749514; PubMed Central PMCID: PMCPMC8806218.

64. Kouroupis D, Best TM, Kaplan LD, Correa D, Griswold AJ. Single-Cell RNA-Sequencing Identifies Infrapatellar Fat Pad Macrophage Polarization in Acute Synovitis/Fat Pad Fibrosis and Cell Therapy. Bioengineering (Basel). 2021;8(11). Epub 20211029. doi: 10.3390/bioengineering8110166. PubMed PMID: 34821732; PubMed Central PMCID: PMCPMC8615266.

65. Hsueh MF, Zhang X, Wellman SS, Bolognesi MP, Kraus VB. Synergistic Roles of Macrophages and Neutrophils in Osteoarthritis Progression. Arthritis Rheumatol. 2021;73(1):89-99. Epub 20201117. doi: 10.1002/art.41486. PubMed PMID: 32783329; PubMed Central PMCID: PMCPMC7876152.

66. Lieberthal J, Sambamurthy N, Scanzello CR. Inflammation in joint injury and post-traumatic osteoarthritis. Osteoarthritis Cartilage. 2015;23(11):1825-34. doi: 10.1016/j.joca.2015.08.015. PubMed PMID: 26521728; PubMed Central PMCID: PMCPMC4630675.

67. Haubruck P, Pinto MM, Moradi B, Little CB, Gentek R. Monocytes, Macrophages, and Their Potential Niches in Synovial Joints - Therapeutic Targets in Post-Traumatic Osteoarthritis? Front

Immunol. 2021;12:763702. Epub 20211104. doi: 10.3389/fimmu.2021.763702. PubMed PMID: 34804052; PubMed Central PMCID: PMCPMC8600114.

68. Zhang Z, Li L, Yang W, Cao Y, Shi Y, Li X, et al. The effects of different doses of IGF-1 on cartilage and subchondral bone during the repair of full-thickness articular cartilage defects in rabbits. Osteoarthritis Cartilage. 2017;25(2):309-20. Epub 20160920. doi: 10.1016/j.joca.2016.09.010. PubMed PMID: 27662821.

69. Ruan S, Deng J, Yan L, Huang W. Evaluation of the effects of the combination of BMP-2-modified BMSCs and PRP on cartilage defects. Exp Ther Med. 2018;16(6):4569-77. Epub 20180919. doi: 10.3892/etm.2018.6776. PubMed PMID: 30542406; PubMed Central PMCID: PMCPMC6257496.

70. MacDonald L, Alivernini S, Tolusso B, Elmesmari A, Somma D, Perniola S, et al. COVID-19 and RA share an SPP1 myeloid pathway that drives PD-L1+ neutrophils and CD14+ monocytes. JCI Insight. 2021;6(13). Epub 20210618. doi: 10.1172/jci.insight.147413. PubMed PMID: 34143756; PubMed Central PMCID: PMCPMC8328085.

71. Coelho I, Duarte N, Barros A, Macedo MP, Penha-Goncalves C. Trem-2 Promotes Emergence of Restorative Macrophages and Endothelial Cells During Recovery From Hepatic Tissue Damage. Front Immunol. 2020;11:616044. Epub 20210208. doi: 10.3389/fimmu.2020.616044. PubMed PMID: 33628208; PubMed Central PMCID: PMCPMC7897679.

72. Harasymowicz NS, Rashidi N, Savadipour A, Wu CL, Tang R, Bramley J, et al. Single-cell RNA sequencing reveals the induction of novel myeloid and myeloid-associated cell populations in visceral fat with long-term obesity. Faseb j. 2021;35(3):e21417. doi: 10.1096/fj.202001970R. PubMed PMID: 33566380; PubMed Central PMCID: PMCPMC8743141.

73. Li RY, Qin Q, Yang HC, Wang YY, Mi YX, Yin YS, et al. TREM2 in the pathogenesis of AD: a lipid metabolism regulator and potential metabolic therapeutic target. Mol Neurodegener. 2022;17(1):40. Epub 20220603. doi: 10.1186/s13024-022-00542-y. PubMed PMID: 35658903; PubMed Central PMCID: PMCPMC9166437.

74. Hoeft K, Schaefer GJL, Kim H, Schumacher D, Bleckwehl T, Long Q, et al. Platelet-instructed SPP1(+) macrophages drive myofibroblast activation in fibrosis in a CXCL4-dependent manner. Cell Rep. 2023;42(2):112131. Epub 20230218. doi: 10.1016/j.celrep.2023.112131. PubMed PMID: 36807143; PubMed Central PMCID: PMCPMC9992450.

75. Kelly B, O'Neill LA. Metabolic reprogramming in macrophages and dendritic cells in innate immunity. Cell Res. 2015;25(7):771-84. Epub 20150605. doi: 10.1038/cr.2015.68. PubMed PMID: 26045163; PubMed Central PMCID: PMCPMC4493277.

76. Ramachandran P, Dobie R, Wilson-Kanamori JR, Dora EF, Henderson BEP, Luu NT, et al. Resolving the fibrotic niche of human liver cirrhosis at single-cell level. Nature. 2019;575(7783):512-8. Epub 20191009. doi: 10.1038/s41586-019-1631-3. PubMed PMID: 31597160; PubMed Central PMCID: PMCPMC6876711.

77. Prantner D, Nallar S, Richard K, Spiegel D, Collins KD, Vogel SN. Classically activated mouse macrophages produce methylglyoxal that induces a TLR4- and RAGE-independent proinflammatory response. J Leukoc Biol. 2021;109(3):605-19. Epub 20200717. doi: 10.1002/JLB.3A0520-745RR. PubMed PMID: 32678947; PubMed Central PMCID: PMCPMC7855181.

78. Sehgal A, Irvine KM, Hume DA. Functions of macrophage colony-stimulating factor (CSF1) in development, homeostasis, and tissue repair. Semin Immunol. 2021;54:101509. Epub 20211104. doi: 10.1016/j.smim.2021.101509. PubMed PMID: 34742624.

March 22, 2024

Dear Editor:

We would be honored if you would consider our manuscript '**CD206^{+}Trem2^{+} Macrophage Accumulation in the Murine Knee Joint After Injury is Associated with Protection Against Post-Traumatic Osteoarthritis in MRL/MpJ Mice'** for publication in the *Plos One*.

Briefly, this work describes the characterization of the murine immune infiltration/changes in response to traumatic injury, at single cell level, in two strains of mice with varied healing abilities, the C57Bl6 and the MRL/MpJ strains. Most importantly, we show that there are dramatic and distinct differences between these strains and we reveal immune populations and transcriptional differences that are associated with the MRL strain, a strain with extraordinary ability to heal injuries. Our data describes for the first time a comprehensive view of immune subpopulation and shifts longitudinally and reveal that macrophages known to promote healing in other tissues, are also present in the uninjured MRL joint, and are likely to be responsible for the super healer activity. We describe in great detail the molecular profiles that distinguishes subpopulations from each strain and how these subpopulations change transcriptionally in response to traumatic injury. The injury model we utilized, is noninvasive, relevant to human health, and provides an exciting opportunity to study changes in the joint at initial timepoints after the injury, time points that are almost impossible to study in human subjects. Our study is highly relevant to human health, provides a detailed 1st account of strain-specific immune differences at single cell level, and highlights potential new therapeutic opportunities by targeting the immune system in post traumatic osteoarthritis.

This study provides the first account of single cell gene expression changes, associated with the early stages of PTOA development in this TC model in strains of mice with varying healing abilities, and highlights many new candidates that may be further explored as biomarkers or as therapeutic candidates, in future experiments.

Thank you for your consideration.
Sincerely,

Gabriela G. Loots, Ph.D
Professor/Doris Ellison Linn Chair in Bone Biology
Director, Orthopaedic Research Laboratory
UC Davis Department of Orthopaedic Surgery
2700 Stockton Blvd, Rm 2407
Sacramento, CA 95817

916-734-7143 office
925-495-9496 cell
gloots@ucdavis.edu

Figure 1

Click here to access/download;Figure;Figure 1.tif

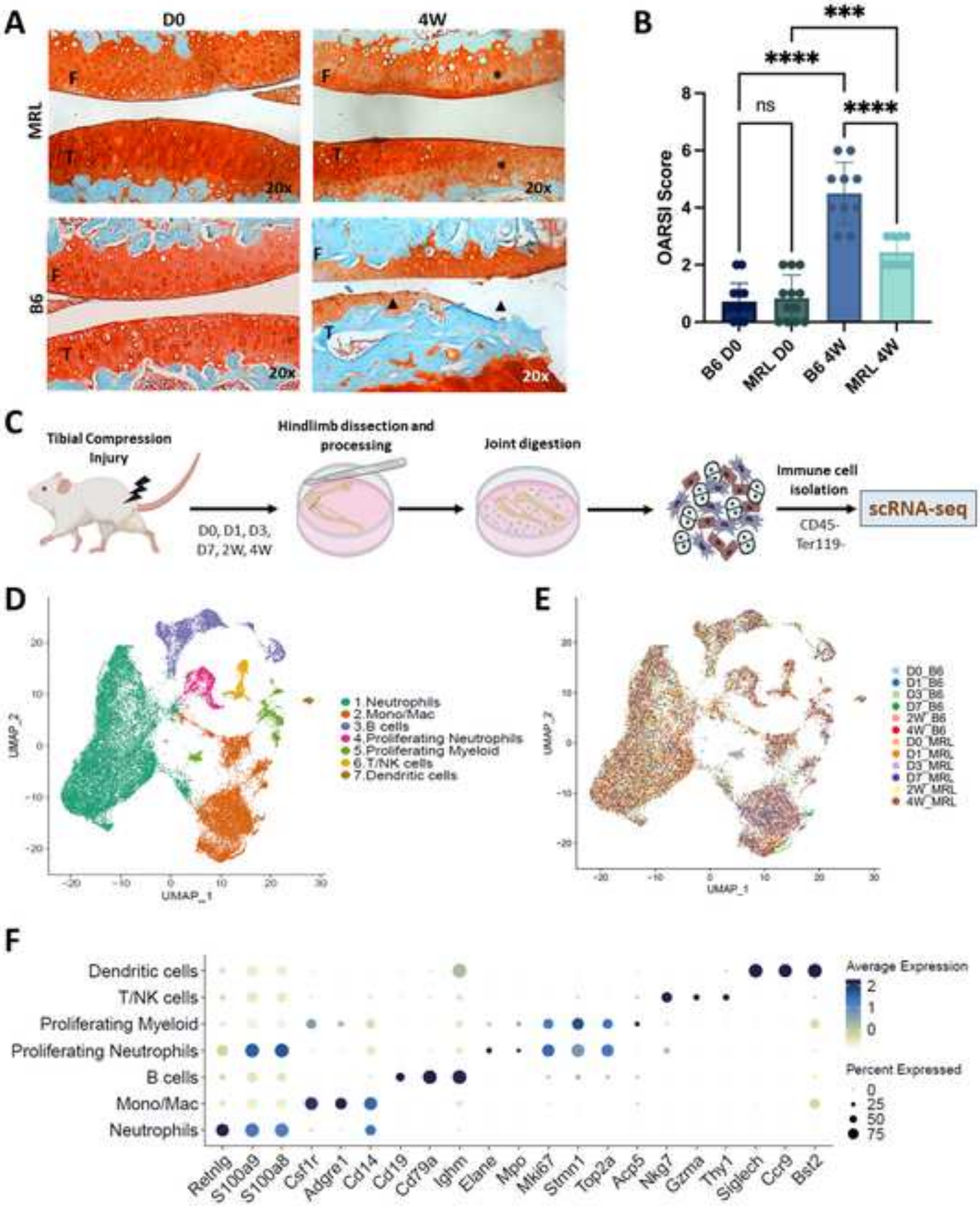

Figure 2

Click here to access/download;Figure;Figure 2.tif

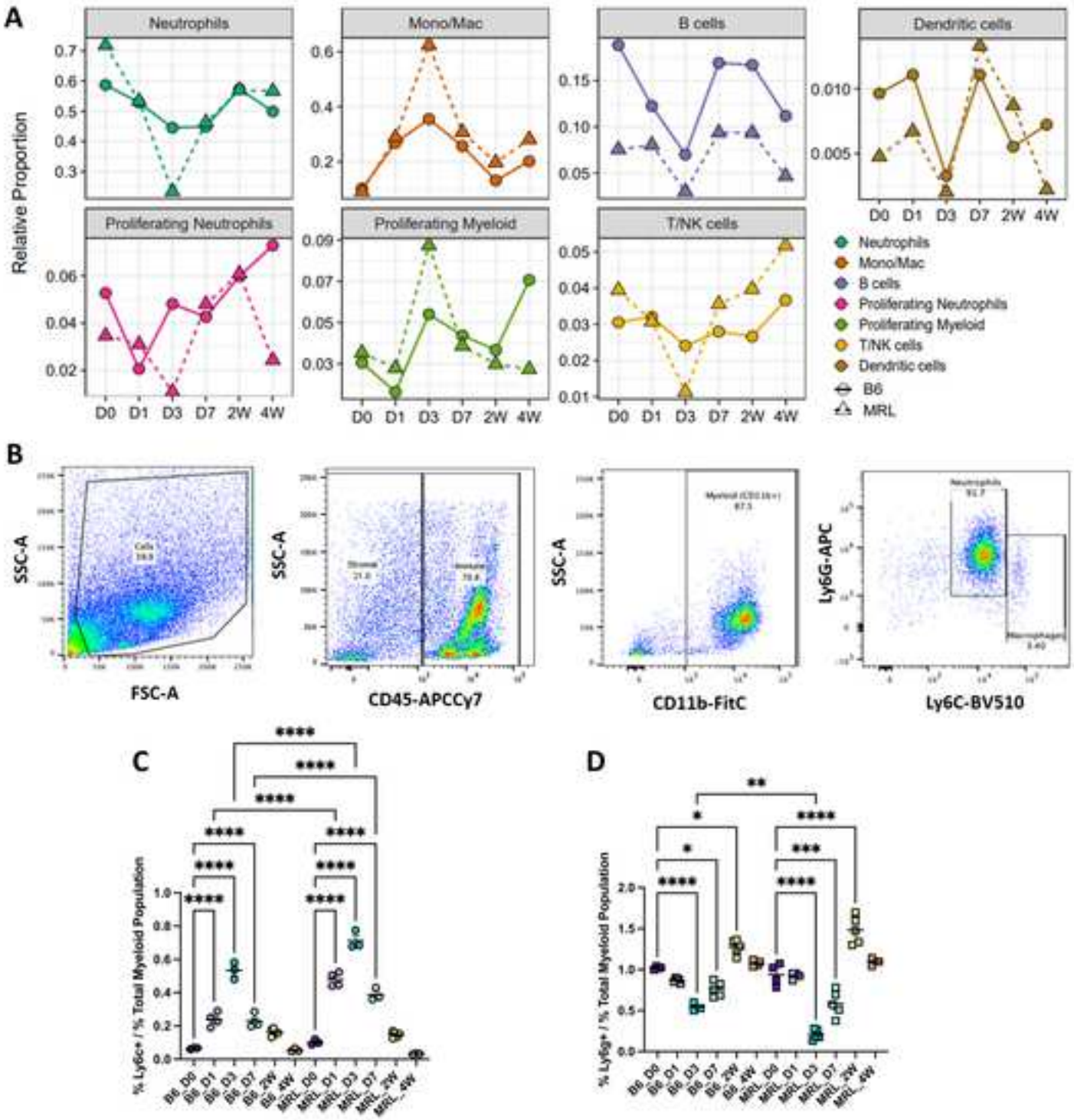

Figure 3

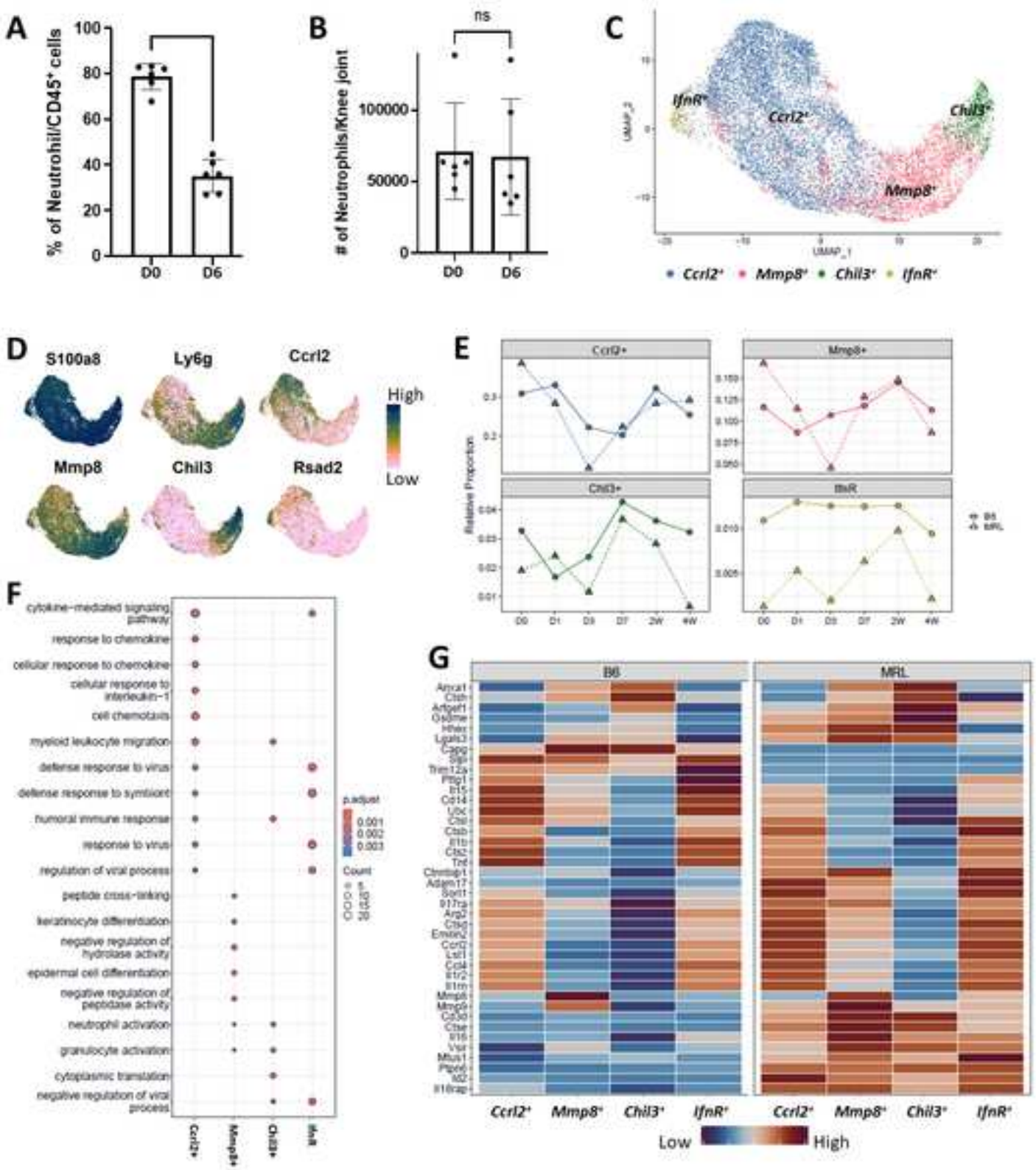

Figure 4

Click here to access/download;Figure;Figure 4.tif

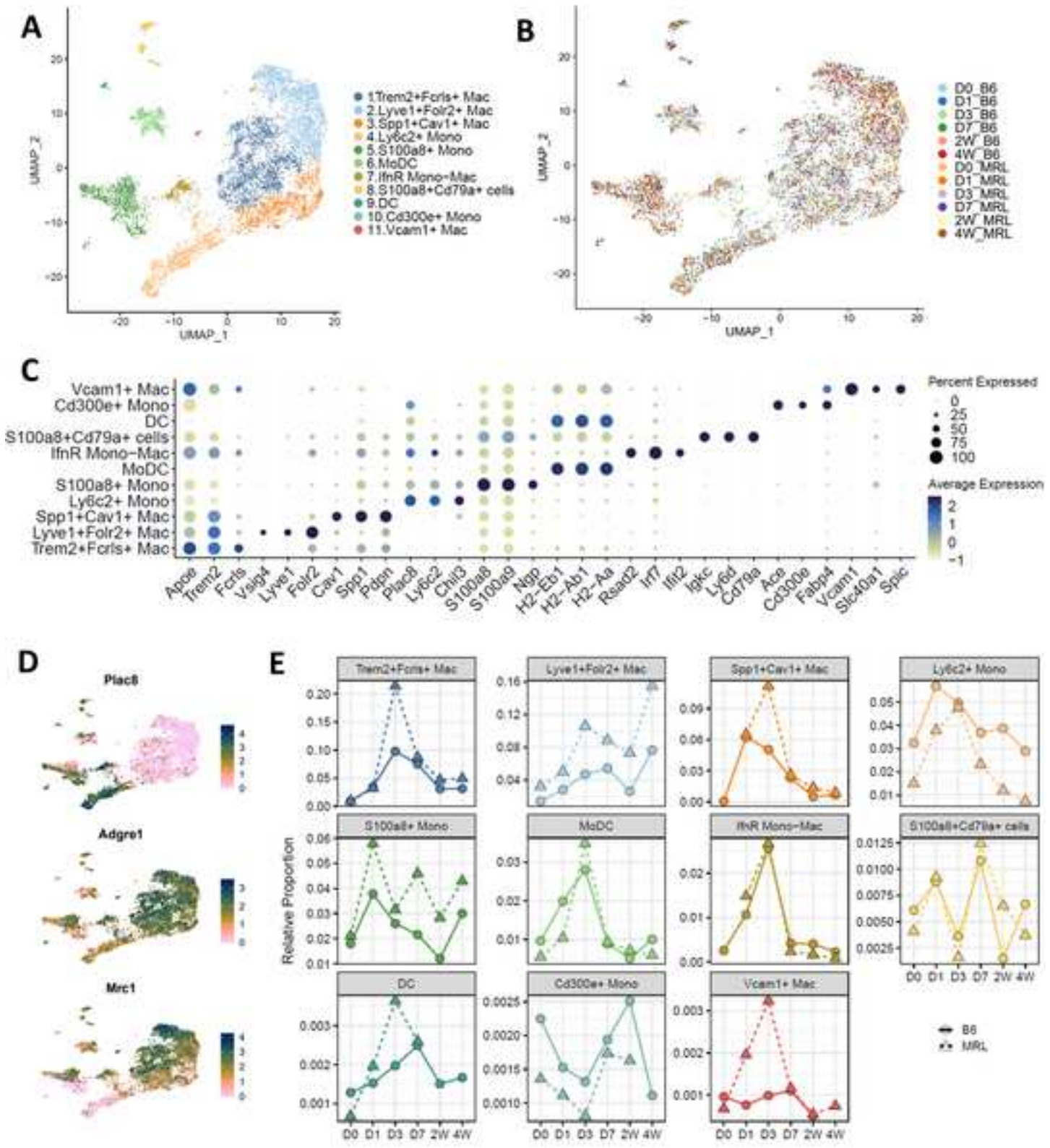

Figure 5

Click here to access/download;Figure;Figure 5.tif

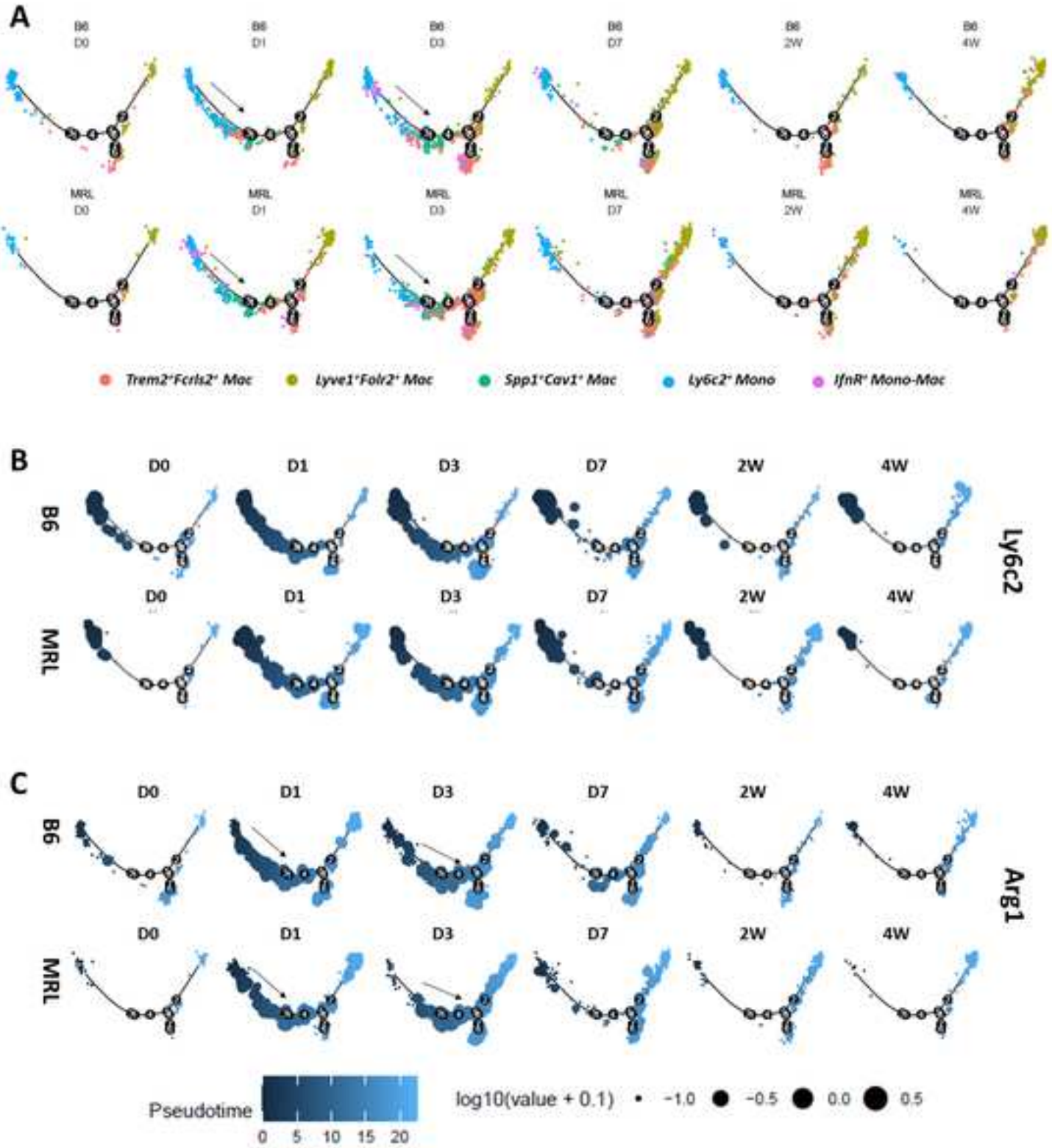

Figure 6

Click here to access/download;Figure;Figure 6.tif

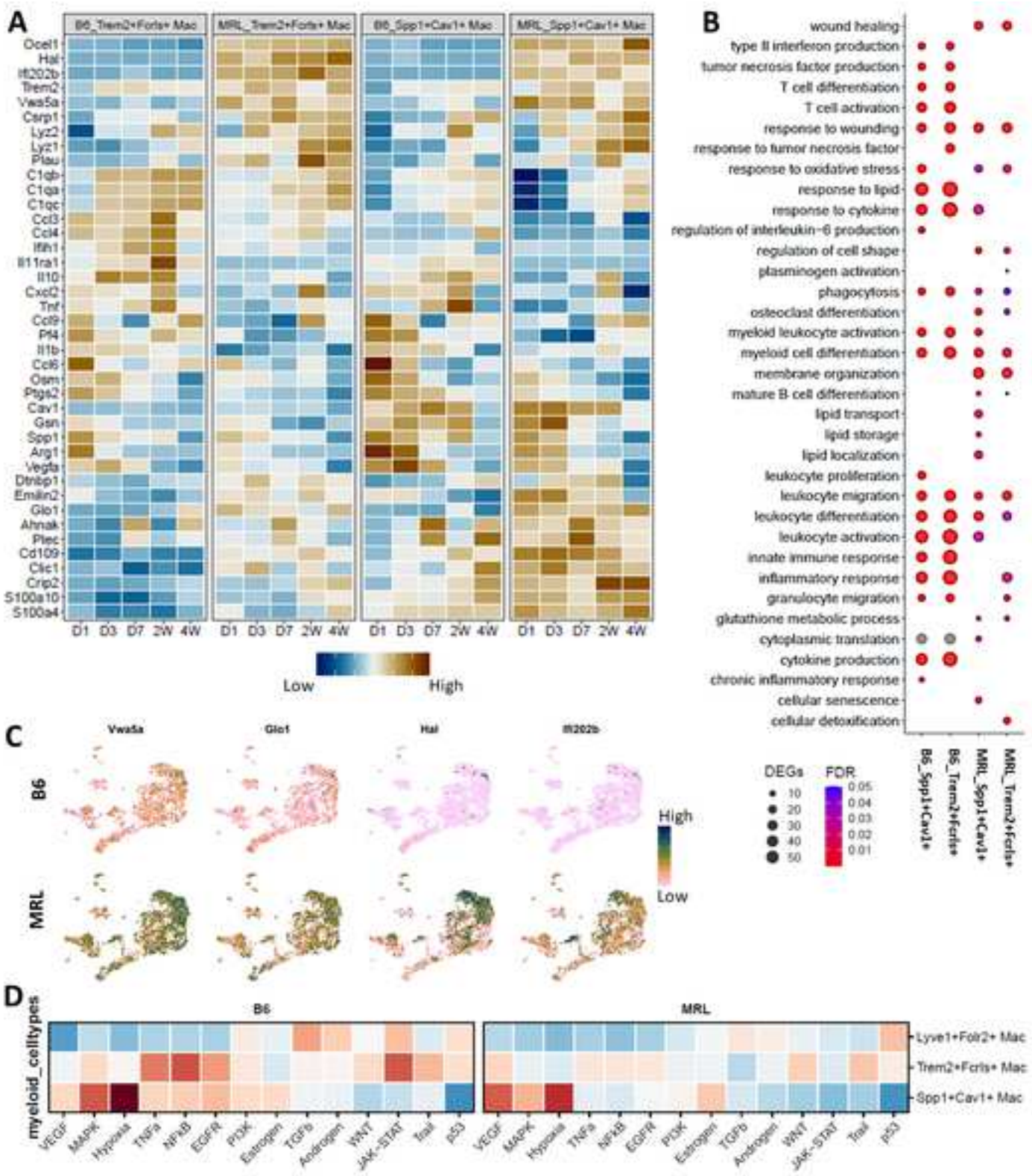

Figure 7

Click here to access/download;Figure;Figure 7.tif

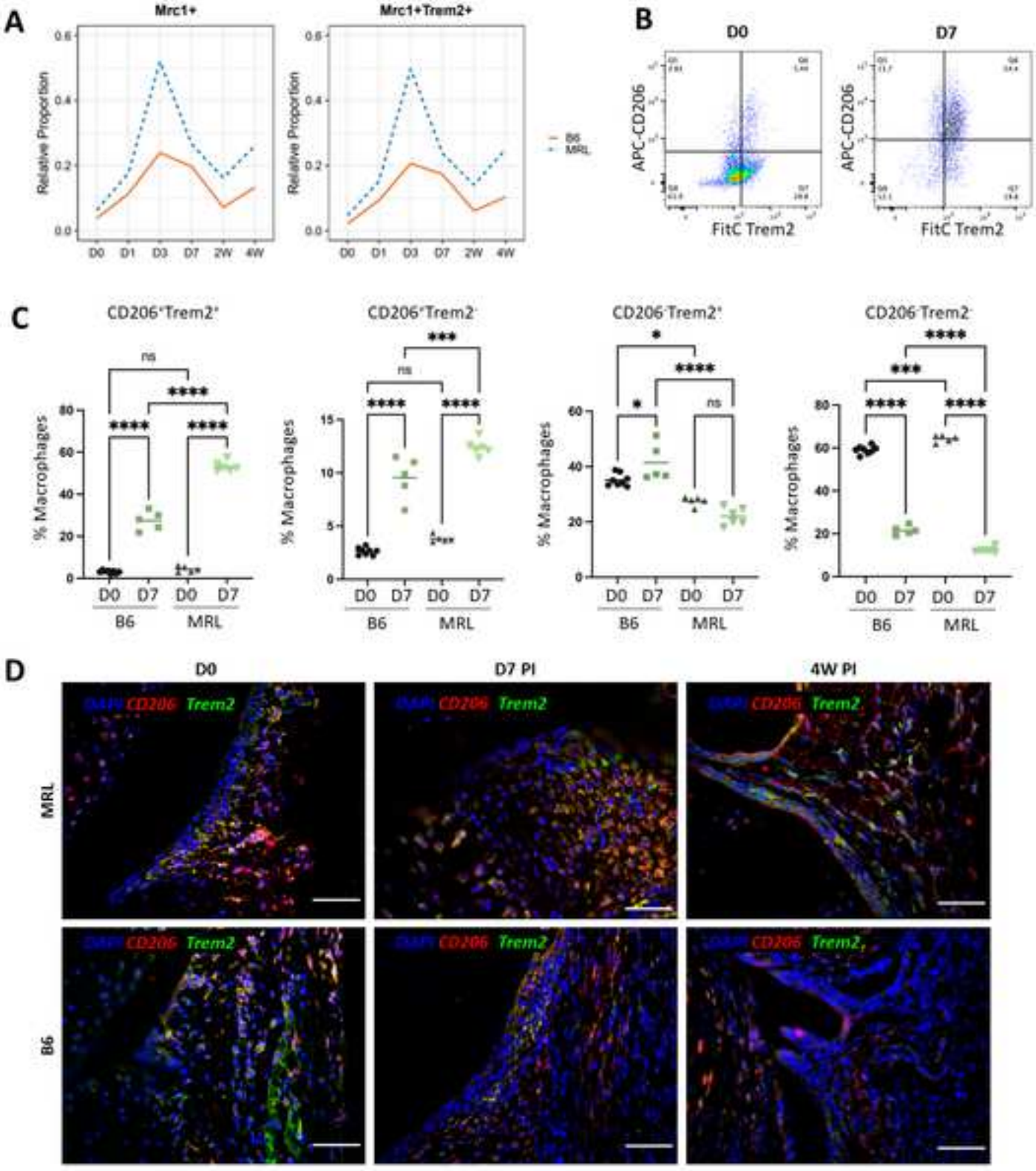

Supplementary Figures

Supplementary Table 1

Click here to access/download

Supporting Information

Table S1.xlsx

Supplementary Table 2

Click here to access/download

Supporting Information

Table S2.xlsx

Supplementary Table 3

Click here to access/download

Supporting Information

Table S3.xlsx

Supplementary Table 4

Supplementary Table 5

Supplementary Table 6

Click here to access/download

Supporting Information

Table S6.xlsx